buildings

MDPI

Article

Generalizable Thermal Performance of Ventilated Block Walls and Energy Implication of Substitution for Wood-Frame Walls in Cold-Climate Buildings

Mohammad Rezvanpour *, Carlos Cruz-Noguez and Yuxiang Chen

Department of Civil and Environmental Engineering, University of Alberta, Edmonton, AB T6G 2R3, Canada; cruznogu@ualberta.ca (C.C.-N.)
* Correspondence: rezvanpour@ualberta.ca

Abstract: Space heating and cooling of buildings is a major contributor to the ascending trend of global energy consumption and greenhouse gas (GHG) emissions. A potential solution to reduce the space heating and cooling is to use buildings' mass for active thermal energy storage (TES). Having air circulation between an active TES and its associated zones can significantly enhance their thermal coupling; however, reported research studies have not focused on this kind of active TES. To that end, this study aimed to evaluate the thermal performance of a ventilated block wall (VBW) in reducing space heating and cooling loads in cold-climate buildings. In this system, air is circulated between a zone and the voided cores of a VBW, where the air exchanges heat with the wall before returning to the zone. To have a generalizable assessment of the system's performance, typical-day and annual energy analyses were conducted under various boundary conditions and air circulation speeds. The study found that for a typical day with significant temperature fluctuation, a VBW with a 2 m/s air circulation speed throughout the day can lead to 67% more net energy exchange (the sum of thermal energy storage and release) when compared to having no air circulation. The annual analysis compared the energy performance between a VBW and a traditional wood-frame wall in three different cold climates. The results showed that substituting a wood-frame wall with a VBW can reduce space heating and cooling loads by 35.1 kWh/m^2 (wall surface area) for a mixed dry–cold climate throughout the year. Having cement plaster as interior finishing can lead to 9% more net energy exchange than having drywall, on average, for all zone air temperature profiles.

Keywords: energy efficiency; cold-climate buildings; space heating and cooling; active thermal energy storage; numerical simulation; ventilated block wall

check for updates

Citation: Rezvanpour, M.; Cruz-Noguez, C.; Chen, Y. Generalizable Thermal Performance of Ventilated Block Walls and Energy Implication of Substitution for Wood-Frame Walls in Cold-Climate Buildings. *Buildings* **2023**, *13*, 1577. https://doi.org/10.3390/buildings13071577

Academic Editor: Antonio Caggiano

Received: 10 May 2023
Revised: 19 June 2023
Accepted: 19 June 2023
Published: 21 June 2023

Copyright: © 2023 by the authors. Licensee MDPI, Basel, Switzerland. This article is an open access article distributed under the terms and conditions of the Creative Commons Attribution (CC BY) license (https://creativecommons.org/licenses/by/4.0/).

1. Introduction

Buildings account for approximately 40% of global energy use and 30% of greenhouse gas (GHG) emissions [1]. Unless strict policies and energy-efficient technologies are adopted, the energy consumption of buildings will continue to increase, posing a serious threat to the global environment and economy [2,3]. Using thermal energy storage (TES) is a cost-effective approach to enhance the energy efficiency of buildings. TES in buildings improves the thermal performance by balancing energy supply and demand, enhancing the use of renewable energy sources (e.g., storing the generated thermal energy from PV panels in the envelope during the day), smoothing zone temperature fluctuations, and improving thermal comfort for occupants [4–7]. Particularly, using a building's envelope (i.e., walls, floor, ceiling) for TES is one of the promising methods. Reduction in heating and cooling demands can be achieved by storing and releasing significant amounts of thermal energy through the thermal mass of the envelope. Storing excess thermal energy in the envelope can buffer zone temperature fluctuations and reduce space heating and cooling loads. The stored heat can then be used later to warm the zone when the indoor temperature drops, such as at night and early in the morning. The process of storing and

releasing heat can be passive, active, or a combination of both strategies. Passive strategies rely on radiation and natural convection on the wall surfaces, while active strategies use mechanical equipment such as fans to circulate heat transfer fluids such as water or air through pipes or channels embedded in the envelope to facilitate the heat exchange. Active TES systems offer several advantages over passive TES systems, including greater control and improved responsiveness. With more precise control over the storage and release of thermal energy, active systems enable better management of energy supply and demand, while their ability to quickly respond to varying environmental conditions and occupants' needs ensures optimal thermal comfort. This improved control and responsiveness leads to higher energy efficiency in buildings, reducing energy consumption and associated costs. Furthermore, enhanced thermal comfort is observed resulting from active TES systems maintaining more consistent indoor temperatures.

The use of active TES as a means of reducing the thermal load of buildings has received significant attention in recent years. In particular, researchers have been studying the use of ventilated block walls (VBWs) as an active TES solution [8–12]. In these types of walls, the hollow cores of the blocks are aligned to create air channels. Circulating air through these channels can accelerate heat transfer as well as thermal energy storage and release. By actively moving air through the channel, the heat transfer rate between the thermal mass and air is increased, allowing for greater storage and release of thermal energy. This increased rate of heat transfer enables the wall to store thermal energy more effectively during periods of high temperature and release it more rapidly during cooler periods. The stored thermal energy in the wall can be released to the zone through the wall surface, outlet air to zone by the use of a fan (i.e., the air is drawn into the channel where it exchanges heat with the wall before being returned back to the zone), or a combination of both. Sources for air ventilation include ambient air, air going to or leaving an air conditioning system, and zone air [8,11]. In the last case, zone air can be drawn into the air channel within the wall, exchange heat with the mass, and then is returned to the zone. One example system is shown in Figure 1. In this system, air circulation can significantly enhance the heat exchange rate (i.e., thermal coupling) between the wall and its surrounding zone, compared to walls without air circulation [8,10].

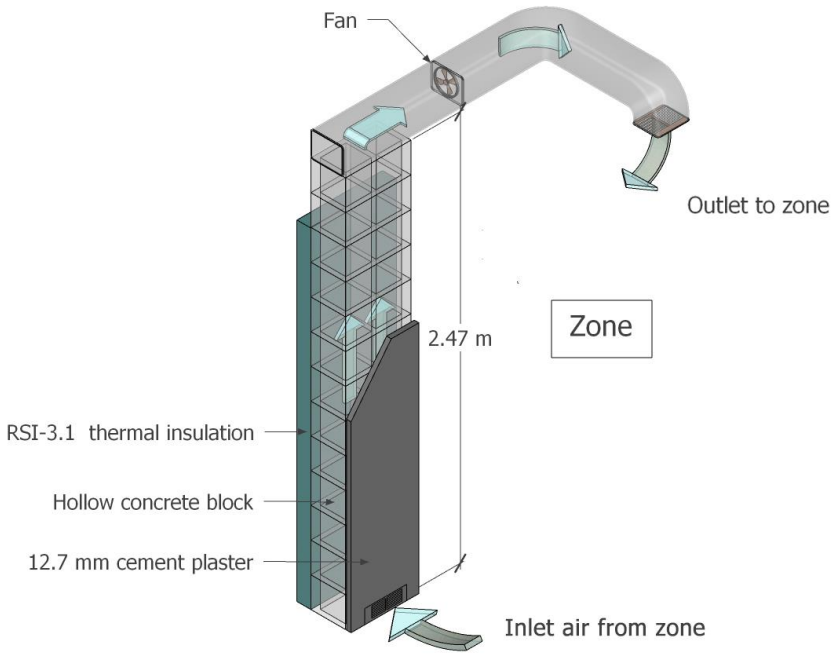


Figure 1. A schematic of the VBW.

The majority of research on using active TES in buildings' mass has focused on ventilated concrete flooring and ceiling slabs [13–18]. A few studies were conducted to

assess the thermal performance of VBWs without outlet air to their associated zones. This type of VBW can be an exterior or interior wall. Huang et al. [10] examined the thermal performance of such an exterior VBW in a hot region in China. The exhaust air from the ventilation system passes through the air channels. Therefore, it was assumed that the temperature of the circulated air would be the same as the indoor temperature. Air circulation enables the wall to store the indoor excess thermal energy during warm periods and release it when the indoor temperature drops. Their findings showed that the impact of channel air speed on the thermal storage performance was much higher than the impact of airflow temperature for a given channel size. The thermal performance of an interior VBW without outlet air to zone was examined in a few studies [11,12,19]. Yu et al. [12] placed and stacked hollow concrete blocks creating a serpentine air channel. Then, they charged the wall with heated air at a constant temperature and speed. The constructed wall was placed in the middle of two identical rooms. A maximum total heat flux density of 112.9 W/m^2 between the wall surface and zone was achieved when the air speed was 2.9 m/s, inlet air temperature was 40 °C, and zone air temperature was fixed at 17 °C.

The benefits of using VBWs that do not have direct outlet air to zone in reducing thermal loads of buildings have been presented in the literature. However, a review of extant literature has shown that there are no studies that have evaluated the performance of VBWs with air circulating between the VBW and its associated zone (referred to as VBW from now on for brevity). VBWs are able to provide dual functionalities, acting as both structural support and thermal energy storage. VBWs enhance building performance through strong thermal coupling with the surrounding spaces and exposing more mass area for heat transfer, promoting effective thermal storage and release. Furthermore, VBWs' simplicity in design and minimal reliance on mechanical equipment make them a cost-effective option for improving the buildings' energy efficiency. Additionally, there is a scarcity of research on the use of VBWs in cold-climate buildings. During the shoulder seasons (spring and fall) in cold climates, buildings experience space heating and cooling within 24-h due to significant fluctuations in weather conditions, resulting in substantial fluctuations in zone temperature. This temperature fluctuation allows VBWs to demonstrate their full potential in thermal energy storage and release.

This study aims to evaluate the typical-day and annual thermal performance of a VBW in a cold region, as shown in Figure 1. The system depicted is designed to effectively exchange heat with its associated zone to prevent space overheating and overcooling, thereby reducing space heating and cooling loads. Throughout the day, as the indoor temperature rises primarily due to solar heat gain and outdoor temperature changes, zone air is directed into the VBW where it exchanges heat with the block mass. The process allows the wall to store excess thermal energy and to cool the air before it is supplied to the zone. This cooled air helps maintain a comfortable temperature and reduces the need for additional cooling. At night and in the early morning, as the indoor temperature drops mainly due to lower outdoor temperature, the zone air takes the stored heat and returns it to the zone. The continuous process of storing and releasing heat ensures a stable indoor temperature and leads to reduction in space thermal loads.

The VBW configuration studied in this research consists of one column of blocks, but more columns can be connected in parallel or series. This study is focused on the thermal performance of a one-column VBW, the height of which equals a typical floor-to-ceiling height of approximately 2.5 m. The performance of multiple columns in parallel will be approximately equal to the one-column performance multiplied by the number of columns.

The VBW illustrated in Figure 1 is constructed by stacking 13 hollow concrete blocks on top of each other [20]. By stacking hollow blocks on top of each other, two air channels are created by connecting the hollow cores. Using a fan, zone air is drawn into each air channel from the bottom and moves upward in the wall height, exchanges heat with the wall, and returns to the zone from the top through a duct. As shown in Figure 1, the modeled VBW consists of a cement plaster finishing on the interior side, hollow concrete blocks, and RSI-3.1 thermal insulation on the exterior side. The choice of RSI-3.1 was made

to meet the minimum standard requirement of RSI-3.5 for exterior walls when combined in series with hollow concrete blocks and cement plaster. In this study, the RSI value for exterior walls was chosen based on the minimum requirement set by the National Energy Code of Canada for Buildings (NECB) in 2020 [21]. The RSI value is a measure of a material's thermal resistance in metric units, with higher values indicating better insulation. Table 1 presents the thermal properties of all layers of the VBW.

Table 1. Thermal properties of the materials used in a VBW.

Materials	Thermal Properties			Refs.
	Thermal Conductivity Coefficient (W/m.K)	Density (kg/m^3)	Specific Heat Capacity (J/kg.K)	
Cement plaster	0.72	1860	840	[22]
Concrete	1.5	2240	840	[22]
Thermal insulation	0.038	25	1400	[23]

The rest of the paper starts with the Methodology (Section 2), consisting of an overview of the performance evaluation in Section 2.1 and the mathematical model in Section 2.2. Section 3 presents the Results and Discussion, which includes an analysis of the typical-day performance in Section 3.1 and the annual energy analysis for both a VBW and wood-frame wall in Section 3.2. The main body of the paper concludes with a summary of the findings in the Conclusions section (Section 4).

2. Methodology

This section elaborates on the research methodology. The first part presents an overview of the types of performance evaluations and explanations of the boundary conditions used for evaluations. The second part of this section describes the mathematical model of the VBW, the heat transfer equations used in the model, and model validation. This part also uses the model to justify the air speed range chosen for performance evaluation.

2.1. Overview on Performance Evaluation

Two types of thermal performance are evaluated: (a) a typical-day performance, which involves an interior and an exterior VBW with outlet air to the zone (referred to as VBW from now on for brevity), and (b) the annual performance, which involves an exterior VBW and an exterior wood-frame wall. The typical-day approach evaluates the 24-h performance across different parameters—zone temperature profiles, air speeds, and interior wall finishes. The parametrized findings can be generalized and applied to a broader range of boundary conditions, through interpolations and extrapolations. Focusing on cold-climate buildings in Canada, the annual energy analysis aims to investigate the yearly performance of the VBW and a traditional wood-frame wall, considering realistic zone temperatures and actual outdoor conditions in three Canadian cities of Edmonton, Vancouver, and Toronto.

2.1.1. Typical-Day Performance

This approach examines the thermal performance of an interior and exterior VBW over the course of a typical day, including the average wall surface temperature, heat flux density, and energy exchange. The "total energy exchange" is represented by a single number and is defined as the cumulative absolute amount of heating and cooling energy that can be supplied to the zone (or absolute variation of thermal energy stored in the VBW) by the VBW during a 24-h period. In this analysis, the zone temperature is assumed to follow a steady-periodic profile. Transient simulations were conducted for a sufficiently long period (i.e., several days) until the wall surface temperature converged. The results of the last 24-h period are used for the typical-day performance. In typical-day analysis,

interior and exterior VBWs are exposed to different boundary conditions. An interior VBW exchanges heat with the zone on both sides. In contrast, an exterior VBW is exposed to outdoor environmental conditions on the outside surface and to the zone on the inside surface. Note that heat exchange only occurs for exterior VBWs on the side exposed to the zone, which is further detailed in the section Heat Loss Percentage Factor.

Zone Temperature Profiles

The thermal performance of a VBW is greatly impacted by its zone temperature profile. To provide a satisfactory level of thermal comfort, various organizations have established minimum and maximum zone temperatures for residential buildings. For this study, Canada was selected as the benchmark country and the temperature range for the zone was set to be between 20 °C and 26 °C [24–28]. A sensitivity analysis of VBW performance was conducted to assess the impact of diverse zone temperature profiles, utilizing typical-day methodology. This sensitivity analysis incorporated a minimum zone temperature of 20 °C, with peak temperatures set at 22 °C, 24 °C, and 26 °C, respectively. A sensitivity analysis reveals how well VBWs perform in terms of reducing the space thermal loads in different ranges of indoor temperatures and air speeds. Variations in outdoor temperature are primarily responsible for indoor temperature swings. Figure 2 illustrates the setup of indoor temperature swings according to the typical fluctuation in outdoor temperature throughout the day. The outdoor temperature is generally lower in the late hours of the night until early morning compared to the rest of the day. In addition, as a result of solar radiation, the outdoor temperature usually rises from late morning until evening. Therefore, the sensitivity analysis evaluated three indoor temperature profiles to determine the impact of temperature variations within the set limits.

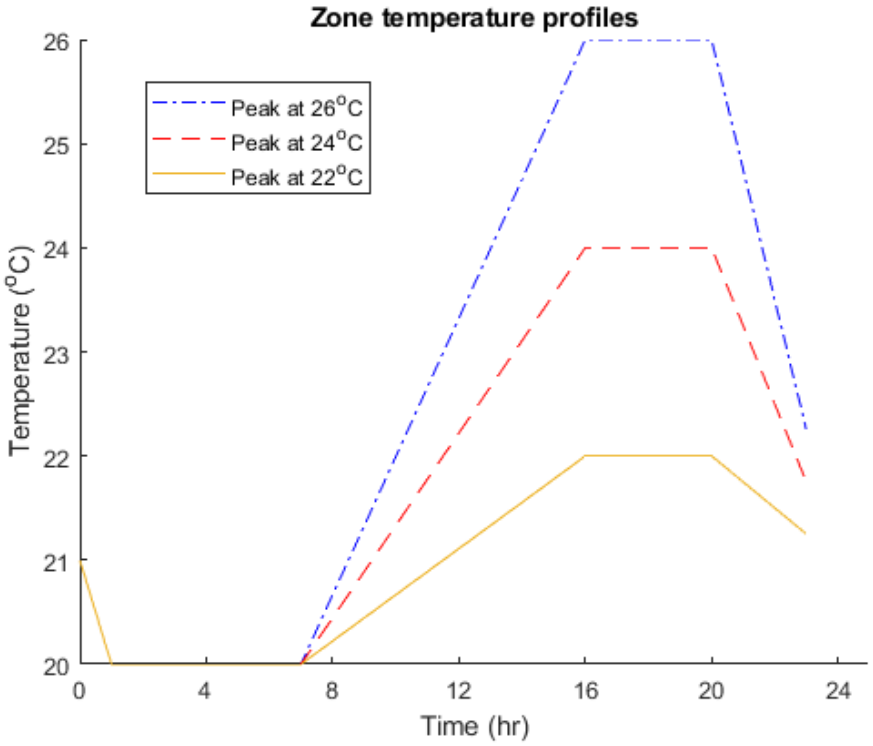


Figure 2. Zone temperature profiles for typical-day performance (a cyclic temperature profile with a 24-h cycle).

Heat Loss Percentage Factor

In cold climates, buildings can experience significant heat loss through their exterior walls when the outdoor temperature drops far below freezing. Therefore, accurately determining the heat loss is crucial when evaluating the thermal performance of a VBW.

Due to the wide range of outdoor temperatures and varying overall thermal resistances, it can be challenging to cover all possible boundary conditions and produce generalizable findings when it comes to exterior walls.

To obtain generalizable findings, this study assumed an adiabatic boundary condition on the exterior surface of the concrete blocks and used a conservative "heat loss percentage" to account for the error due to this assumption. The assumption of an adiabatic boundary condition can be considered accurate in summer due to the thick insulation of exterior walls in cold-climate buildings and insignificant temperature difference between indoors and outdoors. In the case of outdoor temperatures dropping below freezing, there would be significant heat loss through the exterior walls which cannot be ignored. The "heat loss percentage" accounts for heat loss through the exterior wall to the outdoors and applies to the total energy exchange (explained previously) calculated based on the adiabatic boundary assumption. By adopting such an approach, the study aims to provide a comprehensive understanding of wall performance under extreme conditions, thereby offering a more rigorous evaluation of the wall systems' potential in cold-climate buildings throughout the year without considering numerous scenarios for outdoor conditions.

The "heat loss percentage" was determined based on the coldest outdoor temperatures. The heat loss densities from indoors to outdoors through two exterior VBWs, one with no insulation and the other one with an RSI value of 3.5 (minimum overall thermal resistance recommended by NECB [21]), under extremely low outdoor temperatures are shown in Figure 3. The values are simulated with the transient thermal model developed in this study. The model will be described in detail in the following "Mathematical Model" subsection. As shown in Figure 3, at any given point during the day, the heat loss through an insulated wall is approximately 10% of that through an uninsulated one. In other words, the insulated wall keeps 90% of the heat. Since an adiabatic wall would keep 100% of the heat, this means that the insulated VBW loses approximately 10% of the thermal energy that could be stored by an adiabatic wall. The 10% value is the "heat loss percentage" in this study and used to factor the total energy exchange results obtained based on an adiabatic exterior surface. The calculated heat loss percentage of 10% in the typical-day performance analysis is notably conservative, resulting in an underestimated performance throughout the day. For annual energy analysis, the exterior wall is not assumed to be adiabatic, and its behavior is influenced by outdoor temperature fluctuations.

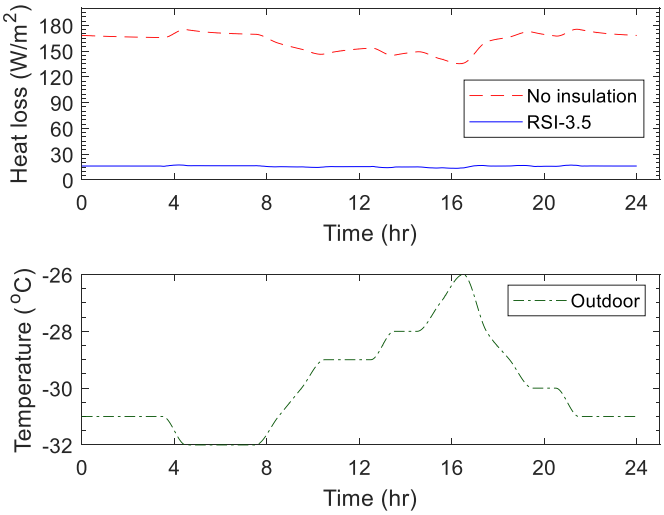


Figure 3. Heat loss values for VBW.

2.1.2. Annual Energy Analysis

The annual energy analysis aims to quantify and compare the yearly impacts of VBWs and traditional wood-frame walls on space heating and cooling loads for three different cold climates. Three Canadian cities—Edmonton, Vancouver, and Toronto—were selected

to represent different cold climates. Edmonton has long, cold winters and short, warm summers, while Toronto has mild temperatures with hot summers and cold, snowy winters. Vancouver enjoys a temperate climate due to its proximity to the Pacific Ocean. The yearly performance of the two wall systems is simulated under a zone temperature profile estimated based on the data from a real house in a similar type of construction and under the outdoor environmental conditions of the three cities (to be detailed in the following paragraphs). The annual energy analysis employs typical meteorological year (TMY) data from 1996 to 2015. TMY is a compilation of selected meteorological data for a specific location over the course of one year. In order to evaluate the thermal performance of a VBW versus a traditional wood-frame wall, two indicators of performance were introduced: assisting heating energy and assisting cooling energy. These indicators refer to the amount of thermal energy stored in a wall that contributes to reduced space heating and cooling loads over the course of a year. Appendix A provides more details about the modeled wood-frame wall.

Table 2 outlines the scenarios and their criteria use assisting heating and cooling energy (kWh/m^2 of the wall surface) for both walls. Notably, one scenario was considered for assisting heating energy, while two scenarios were used for assisting cooling energy. The heating scenario is met when outdoor temperature is lower than the zone temperature and the wall surface temperature is higher. Cooling scenario #1 happens when outdoor temperature is higher than the zone temperature and the wall surface temperature is lower, resulting in the wall cooling the zone. Cooling scenario #2 broadens scenario #1 by using an outdoor temperature greater than 20 °C. In both cooling scenarios, if the wall surface temperature is lower than the zone temperature, assisting space cooling occurs. Cooling scenario #2 involves a broader range of conditions for calculation, resulting in larger values than scenario #1. Furthermore, to prevent unwanted cooling in the zone during the winter, the air circulation is turned off when the temperature of the walls falls below 20 °C. Otherwise, a 2 m/s air speed is maintained for ventilation.

Table 2. Criteria used for calculating the assisting heating and cooling energy.

Scenario	Criteria
Heating (H)	$T_{outdoor} < T_{air} < T_{wall}$
Cooling scenario #1 (C #1)	$T_{wall} < T_{air} < T_{outdoor}$
Cooling scenario #2 (C #2)	$20°C < T_{outdoor}$ $T_{wall} < T_{air}$

Zone temperature greatly affects the thermal behavior of wall systems. The zone temperature at any time depends on the zone temperature at the preceding time. In addition to preceding zone temperatures, outdoor temperature and solar radiation also have a continuous influence on the temperature of a zone. Conducting whole building thermal simulations can yield zone temperature profiles and related wall performance data. However, this approach is limited to the specific building characteristics chosen (e.g., physical construction, room temperature settings, and wall placement) as well as the prevailing climate conditions. To overcome this limitation, this study aims to establish a performance envelope for VBWs and wood-frame walls using a parametric analysis. By incorporating zone temperature as one of the parameters, the study bypasses the need for time-consuming whole-building thermal simulations. Estimating wall performance across a spectrum of outdoor and zone temperatures allows for interpretation and application to a wider array of zone conditions. To obtain a realistic zone temperature profile under varying outdoor conditions, the measured outdoor temperature and GHI data for the EcoTerra

house (located in Eastman, QC, Canada) [29] were used to develop prediction function Equation (1) for zone temperature.

$$T_{air}^{t} = (0.72 * T_{air}^{t-1}) + \left(0.03 * T_{outside}^{t-1}\right) + \left(0.0005 * GHI^{t-1}\right) + \left(0.01 * T_{outside}^{t}\right) + \left(0.0004 * GHI^{t}\right) + 6.4;\ 20 \leq T_{air}^{t} \leq 26 \quad (1)$$

where T_{air}^{t} is the zone temperature in the current timestep (10 min in this study) in °C, T_{air}^{t-1} denotes the zone temperature in the past timestep, GHI^{t} and GHI^{t-1} stand for the global horizontal irradiance in the current and past timesteps in W/m^2, respectively, and $T_{outside}^{t}$ and $T_{outside}^{t-1}$ are the outdoor temperatures in the current and past timesteps in °C, respectively.

Based on Equation (1), the indoor temperature data in the current timestep were chosen as the dependent variable, while the indoor temperature in the past timestep, outdoor temperature in the current and past timestep, and also GHI in the current and past timestep were considered as independent variables. Moreover, the impact of outdoor temperature and solar radiation in the current timestep has been considered in order to minimize the response delay in the predicted temperature.

The goodness of fit was assessed by calculating the R-square parameter, which indicates how well independent variables explain variations in the dependent variable. An R-square of 0.952 was obtained for the comparison between the measured (from EcoTerra house) and predicted indoor temperature, implying that the proposed function can predict the indoor temperature with an acceptable level of accuracy. The comparison between the predicted indoor temperatures and the actual indoor measurements at EcoTerra house for selected days is shown in Appendix B.

This prediction function is used to predict the temperature of a zone located in the three chosen climates/cities with corresponding meteorological data. EcoTerra serves as an exemplary case study due to its combination of heavy thermal mass and wood-frame walls within the same house. This coexistence of both wall systems allows for a direct comparison of their performance under the same conditions, making the analysis more accurate and reliable. Using real data from the EcoTerra house improves the accuracy of predicting zone temperatures, making the performance analysis more reliable. This also strengthens our study's usefulness in understanding how these wall systems work in real-life situations.

2.2. Mathematical Model

As shown in Figure 1, thermal models are developed for a wall strip (i.e., one block width with a 2.47 m height) using the following assumptions and considerations for boundary conditions and heat transfer equations.

2.2.1. Heat Transfer Equations

Figure 4 illustrates a schematic cross-section of the air channel, displaying all of the involved heat transfer mechanisms. As depicted in Figure 4, heat is transferred between air inside the channel and the surrounding wall via convection. Heat is also transferred between the wall nodes facing each other in the channel through radiation. Additionally, the air returning to the zone exchanges heat with the zone air through advection. Advection is a type of convective heat transfer mechanism resulting from the intensive bulk movement of air. The zone also conducts heat transfer with the wall surface through both convection and radiation.

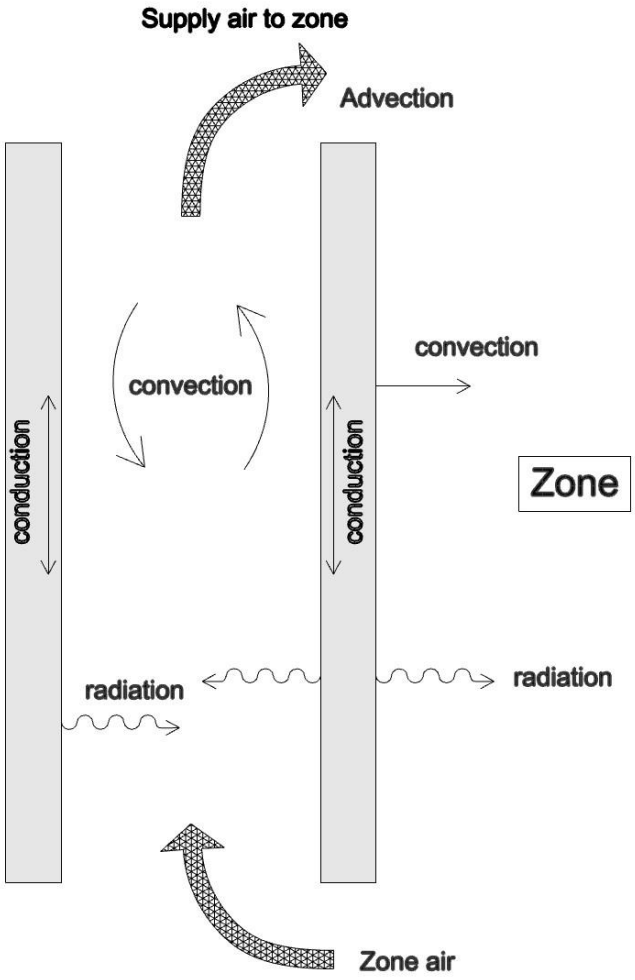


Figure 4. Heat transfer mechanisms in VBWs.

Heat Transfer Inside the Air Channel

The temperature of air inside the channel can be determined by solving Equation (2).

$$(\rho \mathrm{Cp})_{\mathrm{air}}(\mathrm{A_{AC}}\Delta y)\frac{dT^{\mathrm{f}}_{AC}}{dt} = \sum_{m}(h_{air}\mathcal{L}^{i,j,k}\Delta \mathrm{y}\left(T^{i,j,k}_{wall} - T^{\mathrm{f}}_{AC}\right)) - \dot{m}\mathrm{Cp_{air}}\left(T^{\mathrm{f}}_{AC} - T^{\mathrm{f}-1}_{AC}\right) \quad f = 1, 2, 3, \ldots, n_{air} \tag{2}$$

In Equation (2), ρ_{air} and $\mathrm{Cp_{air}}$ represent the density and specific heat capacity of the air inside the channel, respectively. A_{AC} and Δy are the cross-sectional area of the air channel and the height of each control volume (CV) that corresponds to node f, respectively. The indices i, j, k, and f denote the node counters for the wall in three directions (corresponding to Δx, Δy, Δz) and for the air within the channel. In Equation (2), i, j, k are the node coordinates of the wall that is in contact with node f of the air. Furthermore, the summation index m refers to the number of wall nodes surrounding the air node. T_{wall}, T_{AC}, $\dot{m}$, h_{air}, and $\mathcal{L}$ denote the wall temperature, air temperature inside the channel, air mass flow rate, the convective heat transfer coefficient of the air inside the channel, and the length of each CV (either in Δx direction or Δz direction) in contact with node f of air inside the channel, respectively. h_{air} can be determined using Equation (3).

$$h_{air} = \frac{Nu \times \lambda_{air}}{D_h} \tag{3}$$

where D_h, λ_{air}, and Nu are hydraulic diameter, air thermal conductivity, and Nusselt number, respectively. The Nusselt number varies depending on the flow regime (i.e., laminar or turbulent). Equations (4) and (5) determine the Nusselt number [30].

$$Nu = 4.364 \text{ (Laminar flow; } Re_D \leq 2300) \tag{4}$$

$$Nu = \frac{\frac{F_{fr}}{8}(Re - 1000)Pr}{1 + 12.7\left(\frac{F_{fr}}{8}\right)^{0.5}\left(Pr^{2/3} - 1\right)} \left(\text{Turbulent flow; } 3000 \leq Re_D \leq 5 \times 10^6 \text{ \& } 0.5 \leq Pr \leq 2000\right) \tag{5}$$

Re represents the Reynolds number, Pr denotes the Prandtl number, and F_{fr} is the friction factor. Equations (6)–(8) can be used to calculate Re, Pr, and F_{fr} [30,31].

$$Re_D = \frac{v \times D_h}{\vartheta} \tag{6}$$

$$Pr = \frac{\vartheta}{\frac{\lambda_{air}}{(\rho C p)_{air}}} \tag{7}$$

$$\frac{1}{\sqrt{F_{fr}}} = -2log\left(\frac{\epsilon}{3.7D_h} + \frac{2.51}{Re_D\sqrt{F_{fr}}}\right) \tag{8}$$

where v is the air speed, ϑ is the kinematic viscosity, and ϵ is the roughness which was set at 0.3 mm [32].

Heat Transfer between Wall Nodes

Figure 5 illustrates a schematic of the block, showing its dimensions, discretization, and nodes.

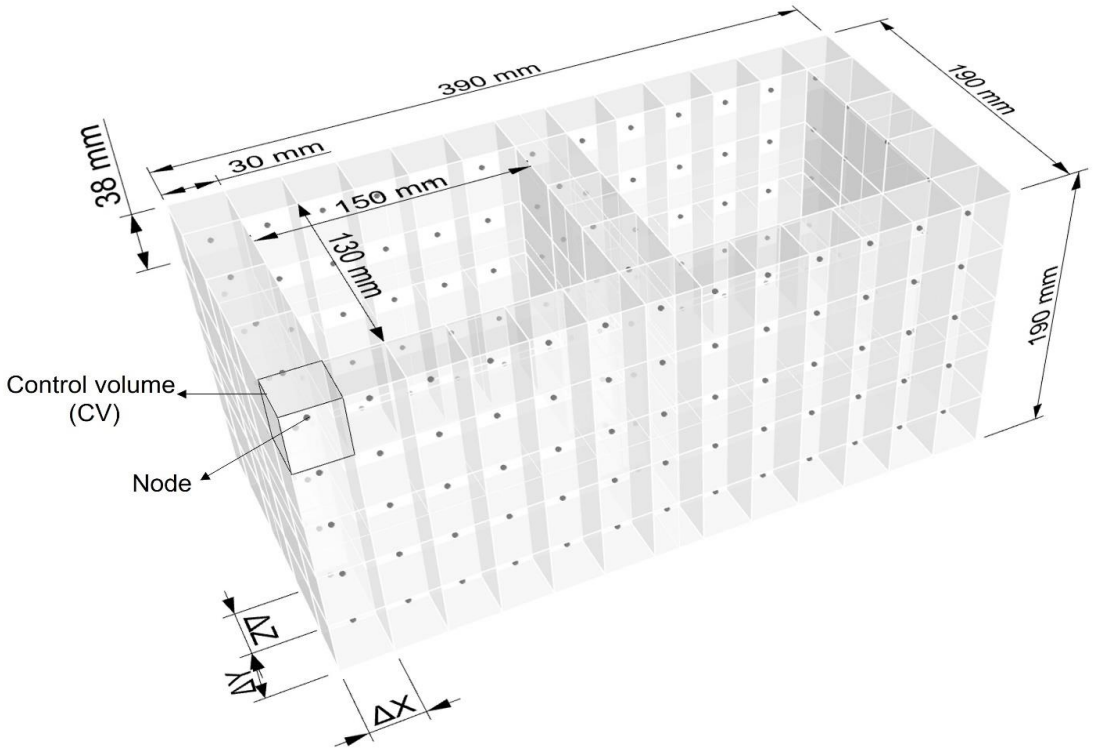


Figure 5. A schematic of the block dimensions, discretization, and nodes.

As shown in Figure 5, the block is discretized equally in three directions with nodes spaced by 30 mm in the x direction and 38 mm for the y direction. In the z direction, the block CVs in the face shells have a width of 30 mm, while the block CVs in contact with air inside the channel have a width of $\frac{130}{3}$ mm. The discretization of other continuous layers such as the cement plaster and rigid thermal insulation mirrors that of the block. Additionally, the dimensions of the block are selected based on those commonly used in construction [20].

Heat transfer between the wall nodes takes place through conduction, convection with the air inside the channel, radiation between wall nodes that are exposed to air and are facing each other, and also the convection heat transfer between the wall surface nodes and the zone air. The latter will be discussed further in the section Heat Transfer between the Wall and Zone Air. The overall impact of all input and output heat flux densities continuously alters the temperature of the CVs. The wall temperature at any given location (i.e., nodes) can be determined by using Equation (9) while considering all heat flux densities entering and exiting the CVs.

$$(\rho Cp)_{wall} V_{wall}^{i,j,k} \frac{dT_{wall}^{i,j,k}}{dt} = Q_{conduction}^{i,j,k} + Q_{convection}^{i,j,k} + Q_{radiation}^{i,j,k} + Q_{surface}^{i,j,k} \quad (9)$$

where V_{wall} represents the volume of each CV, Δx, Δy, Δz are length, height, and width of the CVs as shown in Figure 5, $Q_{convection}$ is the exchanged heat flow rate between air inside the channel and surrounding wall nodes, $Q_{surface}$ denotes the heat flow rate from the zone towards the nodes on the wall surface, $Q_{radiation}$ is the radiation heat flow rate between two facing wall nodes in contact with air, and $Q_{conduction}$ represents the conduction heat flow rate between the wall nodes, which can be calculated using Equation (10).

$$Q_{conduction}^{i,j,k} = \lambda_{\text{wall}} \times \left\{ \begin{array}{l} \frac{\Delta z \Delta y}{\Delta x}\left(T_{wall}^{i+1,j,k} + T_{wall}^{i-1,j,k} - 2T_{wall}^{i,j,k}\right) \\ +\frac{\Delta z \Delta x}{\Delta y}\left(T_{wall}^{i,j+1,k} + T_{wall}^{i,j-1,k} - 2T_{wall}^{i,j,k}\right) \\ +\frac{\Delta y \Delta x}{\Delta z}\left(T_{wall}^{i,j,k+1} + T_{wall}^{i,j,k-1} - 2T_{wall}^{i,j,k}\right) \end{array} \right\} \quad (10)$$

$Q_{convection}$ and $Q_{radiation}$ can be calculated using Equations (11) and (12), respectively.

$$Q_{convection}^{i,j,k} = h_{air} \mathcal{L}^{i,j,k} \Delta y \left(T_{wall}^{i,j,k} - T_{air}^{\text{f}}\right) \quad (11)$$

$$Q_{radiation}^{i,j,k} = \sigma \Delta y \mathcal{L}^{i,j,k} F_v F_\varepsilon \left(T_{wall}^4 - T\prime_{wall}^4\right) \quad (12)$$

where σ is the Stefan–Boltzmann constant (i.e., 5.67×10^{-8} W/m^2.K^4) and F_ε is the emissivity factor (i.e., $F_\varepsilon = \frac{1}{\frac{2}{\varepsilon}-1}$ for ε = 0.85). At each height, the surfaces of the nodes on the same interior surface of the air channel, consisting of three nodes in the Δz direction and five nodes in the Δx direction, are combined to form one surface for radiant heat transfer calculation. $\left(T_{wall} - T\prime_{wall}\right)$ is the difference between average temperature of every two combined interior surfaces of the channel for every Δy (i.e., 38 mm). F_v represents the view factor between two combined surfaces at the same or different heights [30,33]. The view factor between two facing surfaces (on the opposite side of the air channel) can be obtained using Equation (13) [30].

$$\mathcal{F}_{facing} = \frac{2}{\pi \bar{X} \bar{Y}} \left\{ \ln\left[\frac{\left(1+\bar{X}^2\right)\left(1+\bar{Y}^2\right)}{1+\bar{X}^2+\bar{Y}^2} \right]^{0.5} + \bar{X}\left(1+\bar{Y}^2\right)^{0.5} tan^{-1} \frac{\bar{X}}{\left(1+\bar{Y}^2\right)^{0.5}} + \bar{Y}\left(1+\bar{X}^2\right)^{0.5} tan^{-1} \frac{\bar{Y}}{\left(1+\bar{X}^2\right)^{0.5}} - \bar{X} tan^{-1} \bar{X} - \bar{Y} tan^{-1} \bar{Y} \right\} \quad (13)$$

$$\bar{X} = \frac{\Delta y}{d}, \bar{Y} = \frac{W_s}{d}$$

where d is the perpendicular distance between two facing surfaces of the air channel either in the length (Δx) or width (Δz) direction, and W_s denotes the width of each surface. The

view factor for the adjacent surfaces (perpendicular to each other) can be determined using Equation (14).

$$\mathcal{F}_{v-adjacent} = \frac{1 - \mathcal{F}_{v-facing}}{2} \tag{14}$$

Heat Transfer between the Wall and Zone Air

Two mechanisms are involved for the heat transfer between wall and zone air: (a) convection and radiation through the wall surface, (b) advection through the outlet air. Equation (15) can be used to determine the heat transfer between the wall surface and the zone air.

$$Q^{i,j,k}_{surface} = h_{total} \times \Delta y \times \Delta x \left(T^{i,j,k}_{wall} - T_{air} \right) \tag{15}$$

T_{air} is the zone temperature and h_{total} is heat transfer film coefficient (combined convective and radiant heat transfer) between the wall surface and the zone air and other interior zone surfaces. The value for h_{total} can be obtained by solving Equation (16) or Equation (17) depending on the Rayleigh number [22].

$$h_{total} = 1.33 \left(\frac{|T_{air} - T_{wall}|}{H} \right)^{0.25} + 5.5 \qquad 10^5 < Ra < 10^9 \tag{16}$$

$$h_{total} = 1.26 |T_{air} - T_{wall}| + 5.5 \qquad Ra > 10^9 \tag{17}$$

In both Equations (16) and (17), the first term represents the convective heat transfer coefficient, while the constant term represents the radiative heat transfer coefficient [34–36]. H is the wall height and Ra is the Rayleigh number which can be calculated using Equation (18).

$$Ra = GrPr \tag{18}$$

Gr is the Grashof number. Equation (19) can be used to determine the Gr.

$$Gr = \frac{g\beta |T_{air} - T_{wall}| H^3}{(\rho\vartheta)^2} \tag{19}$$

where g and β are the gravitational acceleration and thermal expansion coefficients, respectively. Along with convection and radiation, wall and zone also exchange heat through advection. Equation (20) can be used to determine the heat transfer between outlet air and zone air.

$$Q_{advection} = \dot{m} Cp_{air} \left(T^{\text{f,end}}_{AC} - T_{air} \right) \tag{20}$$

where $T^{\text{f,end}}_{AC}$ is the air temperature at the outlet of the air channel.

2.2.2. Model Validation

Yu et al. [12] investigated the thermal performance of a VBW. They constructed an interior VBW as a common wall between two identical rooms. Heated by an external source, warm air with a fixed inlet temperature and a fixed speed was introduced into hollow-core concrete blocks that were lined up to form serpentine air channels. The wall was ventilated every day between 9 a.m. and 5 p.m. For the remainder of the day, the wall worked naturally. An air conditioner maintained a constant temperature between 17 °C and 18 °C in the zone, although outdoor temperature fluctuations caused variations in the zone temperature. For validation purposes in this study, the developed mathematical model is modified according to the parameters used in the experimental study. Main parameters include the inlet air temperature, air speed, fixed zone temperature, ventilation period (i.e., when air circulation is active and when it is turned off), concrete block dimensions, wall area, and thermal properties of the wall. Furthermore, to represent the error between measured and simulated values, the coefficient variation of the root-mean square error

(CV-RMSE) statistical measure is selected. CV-RMSE can be calculated using Equation (21) [37].

$$CV - RMSE = \frac{\sqrt{\frac{\sum_{i=1}^{n}(y_i - \hat{y}_i)^2}{n}}}{\bar{y}} \quad (21)$$

where n is the number of data points; y_i is the measured value; $\hat{y}_i$ is the simulated value; and $\bar{y}$ is the average of all measured values.

Figure 6 illustrates the simulated and measured average wall surface temperature profiles over the 24-h period. As shown in Figure 6, the simulated wall temperature closely followed the trend of measured wall surface temperature. However, some deviations of up to 0.45 °C were observed, particularly between 10 a.m. and 4 p.m. These deviations could be caused by variations in the inlet air temperatures, speed of air in the channel, and the zone temperature. It is indicated by the CV-RMSE of 1.175% when comparing the model's simulated data (red line in Figure 6) to the actual measured data (blue dotted line in Figure 6) from the experiment. The comparison indicates that the mathematical model developed in this study has sufficient accuracy for simulating the thermal performance of the VBW of interest.

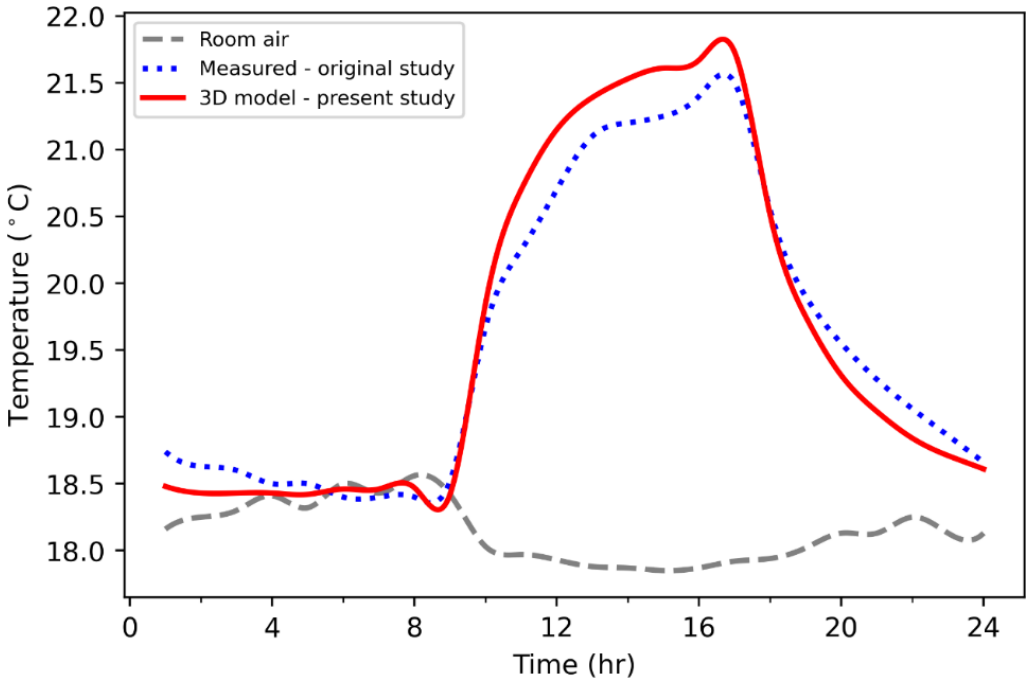


Figure 6. Measured and simulated average wall surface temperatures.

2.2.3. Air Speed in the Air Channel

A major factor influencing the thermal performance of VBWs is the air speed [10]. Reviewed studies reported air speed values ranging from 0.2 m/s to 3 m/s for investigating the thermal performance of ventilated walls [10,12,38–40]. Nevertheless, each case study requires an optimum air speed in accordance with the design, the system's energy consumption (e.g., fan), as well as its net energy exchange. To determine the optimal air speed, the "net energy exchange" was calculated as the difference between total energy exchange from the wall (e.g., sum of the exchanged energy through the surface and the outlet air as explained in the Typical-Day Analysis subsection) and fan energy consumption in a typical-day zone temperature profile with the zone temperature of 26 °C. Net energy exchange is obtained using the model developed in this study.

Equation (22) can be used to obtain the fan energy consumption in a day.

$$E_{fan} = \Delta P \times v \times A_{AC} \times (24/1000) \quad (22)$$

where E_{fan} is the fan energy consumption in kWh, v denotes the air speed in the channel in m/s, and ΔP is the total pressure loss (i.e., static pressure generated by the fan) in Pa. The static pressure provided by the fan can be determined by balancing the channel's static pressure, which includes pressure added by the fan and pressure lost through major head losses caused by friction (minor losses are discussed later). Through this balance, ΔP can be obtained using Equation (23) (Darcy–Weisbach equation) [41].

$$\Delta P = \frac{f \times L}{2D_h} \rho v^2 \quad (23)$$

Different E_{fan} and net energy exchange values are calculated for air speeds ranging from 0.2 m/s to 5 m/s. Figure 7 shows the changes in E_{fan} and net energy exchange based on the different air speeds for a wall strip.

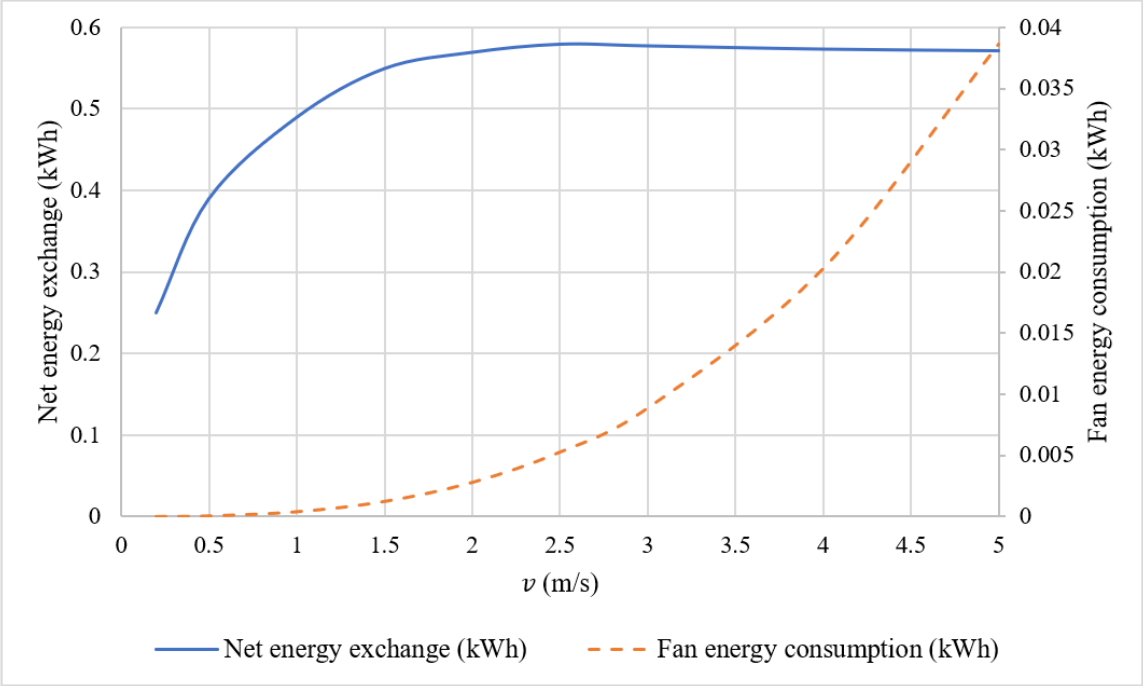


Figure 7. Net energy exchange and fan energy consumption.

Figure 7 depicts that as air speed was increased from 0.2 m/s to 2.5 m/s, the net energy exchange values also increased. However, for speeds above 2.5 m/s, net energy exchange decreased as the rate of fan energy consumption exceeded the rate of energy exchange. Therefore, in order to obtain the maximum net energy exchange, the optimal air speed was determined to be 2.5 m/s. Despite that, simulations were carried out using air speeds of 0 m/s (i.e., passive performance), 1 m/s, and 2 m/s for the parametric analysis. A speed of 2 m/s instead of 2.5 m/s was examined to account for additional minor head losses in the system caused by the inlet and outlet covers of the channel, as well as by the manifold, valves, and elbows in the system.

The air speed in the channel may change depending on the temperature difference between the air at the channel's inlet and outlet. Such variations are caused by changes in air density resulting from alterations in air temperature. Based on the fact that the maximum temperature difference between the inlet and outlet is only ~1.7 °C, resulting in a less than 1% change in air density from inlet to outlet [22], the study assumed that

the volumetric flow rate within the channel remains constant and that the air speed is not affected by such changes in air density from inlet to outlet.

3. Results and Discussion

The results of the two types of performance evaluation are presented in this section as follows:

(a) Typical-day thermal performance of a VBW. This part presents the average wall surface temperature, the heat flux density, the net energy exchange, and the influence of interior finishing on the net energy exchange based on the following boundary conditions and parameters:
   i. Exterior and interior walls;
   ii. Air speeds of 0 m/s, 1 m/s, and 2 m/s;
   iii. Different zone temperature profiles.

(b) In this part, figures and descriptions are presented for a single zone temperature profile (minimum of 20 °C and maximum of 26 °C), an air speed of 2 m/s, and one wall strip. Results for other scenarios are tabulated in their respective sections. Annual energy analysis of a VBW and a wood-frame wall for three Canadian cities is presented.

In this part, the energy performances of both an exterior VBW and exterior wood-frame wall were compared over the course of a year, with a focus on the cold climate of Canada. Specifically, the results and descriptions in this annual energy analysis pertain to the city of Edmonton. Results for other Canadian cities such as Vancouver and Toronto can be found in Appendix C.

3.1. Typical-Day Performance of VBW

The typical-day performance evaluation of an exterior VBW with room air circulation is presented first and followed by that of an interior VBW.

3.1.1. Exterior Wall

Average Wall Surface Temperature

Air speed and zone air temperature fluctuations have a significant impact on average wall surface temperature. In this study, as well as throughout the paper, the term "zone air temperature" is used based on the assumption that the room air and the interior surfaces are at the same temperature. This assumption allows for treating the entire zone as having a single, consistent temperature, which is referred to as the zone air temperature. At an air speed of 2 m/s, Figure 8 illustrates the changes in zone air temperature and average wall surface temperature.

In situations of strong heat exchange between the mass and the zone, the wall surface temperature closely follows the fluctuations in the zone air temperature. This is because the air inside the channel constantly transfers heat between the inner mass of the VBW and the zone. In the case of a wall that is warmer than the zone, as shown in Figure 8 (early in the morning and late at night), the circulating air takes heat from the mass and releases it to the zone. Rapid heat exchange occurs continuously between the wall and zone air, causing the wall temperature to decrease during the following hours, following the zone temperature. The larger difference between the minimum and maximum temperature of the wall indicates more thermal energy storage in the wall and effective heat exchange between the wall and the zone. As a result, further space heating and cooling loads can be reduced as well as establishment of a more stable zone temperature. Similarly, when a wall is colder than the zone (from morning to evening in Figure 8), the process is reversed. In contrast to significant swings in zone air temperature, a situation with insufficient heat exchange will result in a smaller difference between the maximum and minimum wall temperatures. Therefore, the wall is unable to moderate the zone temperature effectively [8].

The zone temperature is predefined in this typical day analysis. However, the actual zone temperature would be different from the predefined values and be affected by the VBW.

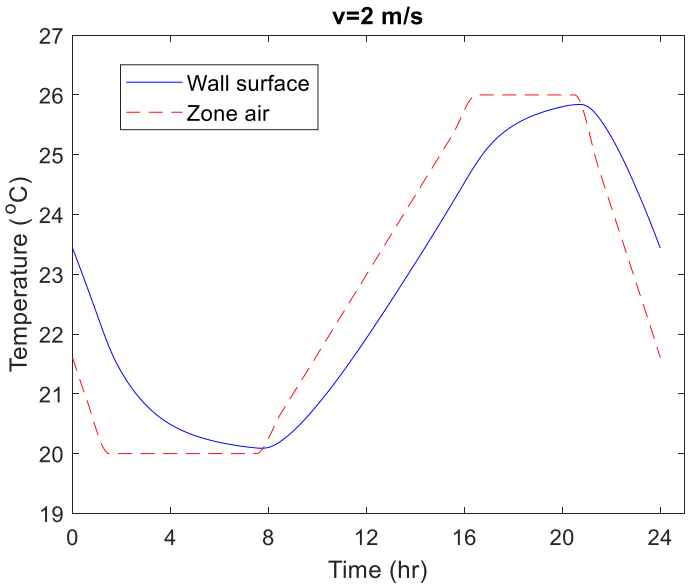


Figure 8. Zone air and average wall surface temperatures for an exterior VBW.

Table 3 presents the minimum and maximum average wall interior surface temperatures, as well as the difference between the maximum and minimum wall surface temperature (which is referred to as ΔT from this point onwards) for different zone temperatures and air speeds.

Table 3. Maximum and minimum average wall interior surface temperatures for different zone temperatures and air speeds.

Zone Temperature (Min/Max) (°C)	Average Wall Surface Temperature (°C)								
	v = 0 m/s			v = 1 m/s			v = 2 m/s		
	Min	Max	Max − Min (ΔT)	Min	Max	Max−Min (ΔT)	Min	Max	Max−Min (ΔT)
20/26	21.21	24.21	3.0	20.44	25.50	5.06	20.10	25.90	5.80
20/24	21.0	23.0	2.0	20.33	23.72	3.39	20.20	24	3.80
20/22	20.40	21.60	1.20	20.31	22	1.69	20.22	22	1.78

According to Figure 8 and Table 3, a higher air speed leads to a stronger heat exchange between the wall and the zone, which results in better moderation of zone air temperature. This is due to the fact that a lower air speed decreases the heat transfer coefficient in the air channel. Thus, less heat is exchanged between the air and the wall, leading to weak heat exchange between the wall and the zone. Additionally, Table 3 shows that a rise in zone peak temperature from 24 °C to 26 °C causes a 31% increase in ΔT for a fixed air speed. Increasing the air speed from 1 m/s to 2 m/s results in a 11% increase in ΔT for a given zone temperature profile. Table 3 reveals that higher temperature fluctuation within the zone has a greater impact on ΔT than increasing air speed.

Heat Flux Density

The heat flux density (q) is defined as the rate of thermal energy (W) exchanged between the VBW and the zone per unit area of the VBW's exposed surface (m^2). A negative heat flux density indicates that the exterior surface or outlet air is cooling the zone at that particular time. In other words, the exterior surface temperature or outlet air

temperature is lower than the zone temperature. Figure 9 illustrates the heat flux density for an air speed of 2 m/s. In Figure 9, "Convection+Radiation" represents the fluctuations in heat flux density between the wall surface and the zone through convection and radiation together. "Advection" solely shows the heat flux density between the outlet air to zone and the zone air.

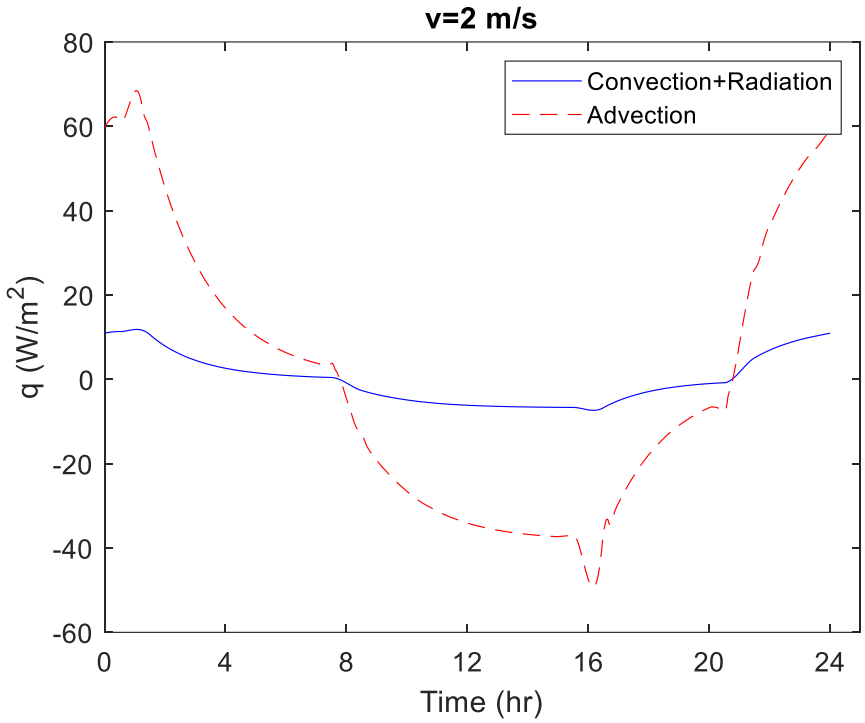


Figure 9. Heat flux density for an exterior VBW over a 24-h period (positive values mean heat flows from the wall to the room).

Figure 9 indicates that the VBW provides heating to the zone from 12 a.m. to 8 a.m. and also from 9 p.m. to 12 a.m. Cooling contributions were from 8 a.m. to 9 p.m. when the zone temperature was on the rise. Equations (15) and (20) can be used to determine the heat flux density through the wall surface (i.e., convection and radiation) and the heat flux density through the outlet air (i.e., advection), respectively. Table 4 presents the minimum and maximum heat flux densities for different zone temperature profiles and air speeds.

Table 4. Heat flux density for exterior VBW with cement plaster.

Zone Temperature (Min/Max) (°C)	Heat Transfer Mechanism	Heat Flux Density (Min/Max) (W/m^2)		
		v = 0 m/s	v = 1 m/s	v = 2 m/s
20/26	Convection and radiation	−14.6/16.3	−9.1/14.1	−6.9/11.1
	Advection	0	−32.6/41.5	−48.6/67.8
20/24	Convection and radiation	−9.6/11.7	−6.1/10.4	−4.3/8.2
	Advection	0	−19.9/40.2	−21.5/52.5
20/22	Convection and radiation	−4.6/7.1	−3.1/6.4	−2.2/5.6
	Advection	0	−10.7/16.7	−16/24.6

Referring to Figure 9 and Table 4, it can be observed that maximum combined convection and radiation heat flux densities decrease with increasing air speed. On the other hand, at elevated air speeds, the maximum advection heat flux densities increase. Increasing the air speed shortens the duration of heat exchange between the circulation air and the wall,

resulting in minimal changes in circulation air temperature. However, higher air speeds significantly enhance the convective heat transfer coefficient within the air channel, resulting in higher rates of heat exchange. When analyzing the heat flux densities within the range of 0 m/s to 2 m/s for air speed, it was discovered that at air speeds lower than 0.3 m/s, convection and radiation are the dominant heat transfer mechanisms when compared to advection.

Net Energy Exchange

The net energy exchange values presented below have been factored by the heat loss percentage of 10%. This percentage (i.e., 10%) is considered conservative because, during the summer months, the temperature difference between indoor and outdoor is insignificant and the heat loss percentage factor would be small.

For walls with more than one column of blocks (same height of 2.47 m), net energy exchange can be determined by multiplying the results for one wall strip by the desired number of block columns. Table 5 presents the net energy exchange for different zone temperature profiles and air speeds. The net energy exchange is calculated by deducting the fan's energy consumption from total energy exchange values.

Table 5. Net energy exchange of the exterior VBW with cement plaster.

Zone Temperature (Min/Max) (°C)	Net Energy Exchange (kWh/m^2)		
	v = 0 m/s	v = 1 m/s	v = 2 m/s
20/26	0.2	0.49	0.57
20/24	0.13	0.33	0.39
20/22	0.06	0.17	0.21

For any given zone temperature profile, increasing the air speed from 0 m/s to 2 m/s increased the net energy exchange by 65%. Furthermore, for any given air speed, increasing the zone peak temperature from 22 °C to 26 °C increased thermal energy storage by 67%. These findings demonstrate the significant impacts of air speed and zone temperature swings on the net energy exchange. The results reveal that significant thermal energy storage can be attributed to the VBW, which in turn leads to efficient diurnal buffering and balancing of a zone's heating and cooling loads. This effectiveness is particularly important during the shoulder seasons (e.g., spring and fall) in cold-climate regions, when zones are more likely to experience substantial temperature fluctuations. Given these benefits, it is seen that VBWs can play a crucial role in maintaining comfortable indoor temperatures and reducing overall thermal loads.

Impact of Interior Finishing Layer on the Thermal Performance

Drywall, also known as gypsum board, and cement plaster have been extensively utilized as interior finishes on wall surfaces and studied in the literature [11,18,42–44]. Adding a layer on top of the interior surface of the wall has an effect on the rate of heat exchange between the zone air and the wall surface. This section examines the impact of three finishing layers, namely drywall, a thermal insulating material, and cement plaster, on the net energy exchange between the zone and the exterior VBW. To assess the impact of a finishing layer on the performance of a VBW, simulations were conducted at both passive performance (i.e., v = 0 m/s) and with an air speed of 2 m/s for all three typical-day zone air temperature profiles. Table 5 shows the simulation results of net energy exchange for the VBW with cement plaster as the interior finishing layer. Appendix D presents the tabulated simulation results for the exterior VBW when drywall is used as the interior finishing layer. The detailed results for the thermal insulating materials are not tabulated, but the general impact is presented below.

Under passive performance, replacing cement plaster with drywall reduced net energy exchange (there is no fan in passive performance) between the wall and the zone air by an

average of approximately 16% across all zone air temperature profiles. When the cement plaster layer was replaced by a layer of thermal insulation, net energy exchange decreased by 45%. This is rooted in the fact that cement plaster has a higher thermal conductivity than the other two materials, allowing it to transfer heat more efficiently through its surface, thereby facilitating better heat exchange between the wall surface and zone air throughout the day. When ventilation is turned on, the contribution of the exposed wall surface decreases. At an air speed of 2 m/s, replacing cement plaster with drywall and thermal insulation decreased net energy exchange by an average of 10% and 16%, respectively, across all zone air temperature profiles. Therefore, the influence of the finishing layer on energy exchange values decreases with increasing air speed.

3.1.2. Interior Wall

Average Wall Surface Temperature

As an interior wall, both sides of the VBW are exposed to the same zone temperature profile. Figure 10 shows changes in average wall surface temperature for an air speed of 2 m/s.

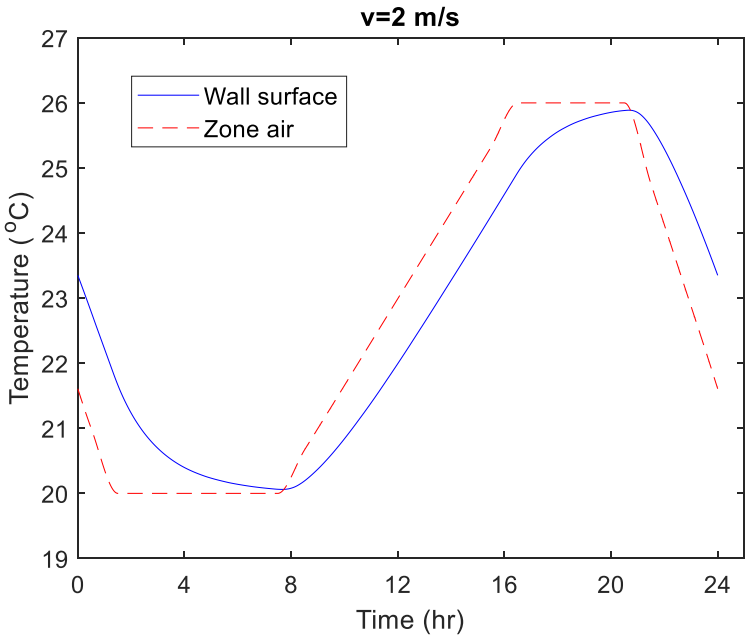


Figure 10. Zone air and average wall surface temperatures for an interior VBW.

Table 6 presents the minimum and maximum interior wall surface temperatures, as well as the difference between the maximum and minimum (ΔT) for different zone temperatures and air speeds.

Table 6. Maximum and minimum average wall interior surface temperatures for different zone temperatures and air speeds.

Zone Temperature (Min/Max) (°C)	Average Wall Surface Temperature (°C)								
	v = 0 m/s			v = 1 m/s			v = 2 m/s		
	Min	Max	Max−Min (ΔT)	Min	Max	Max−Min (ΔT)	Min	Max	Max−Min (ΔT)
20/26	20.93	24.83	3.90	20.26	25.63	5.37	20.05	25.95	5.90
20/24	20.67	23.19	2.52	20.18	23.75	3.57	20.07	23.87	3.80
20/22	20.41	21.6	1.19	20.12	21.88	1.76	20.05	21.94	1.89

According to Figure 10 and Table 6, in an interior VBW, a greater ΔT was observed compared to an exterior VBW. This can be explained by the higher rates of convection and radiation through the surface. The increase in exposed wall surface resulted in a stronger heat exchange between the wall and the zone.

Heat Flux Density

Figure 11 illustrates the change in heat flux density for an air speed of 2 m/s. The exposed surface area of an interior wall would be double that of an exterior wall since the interior wall is exposed to the surrounding zone from two sides.

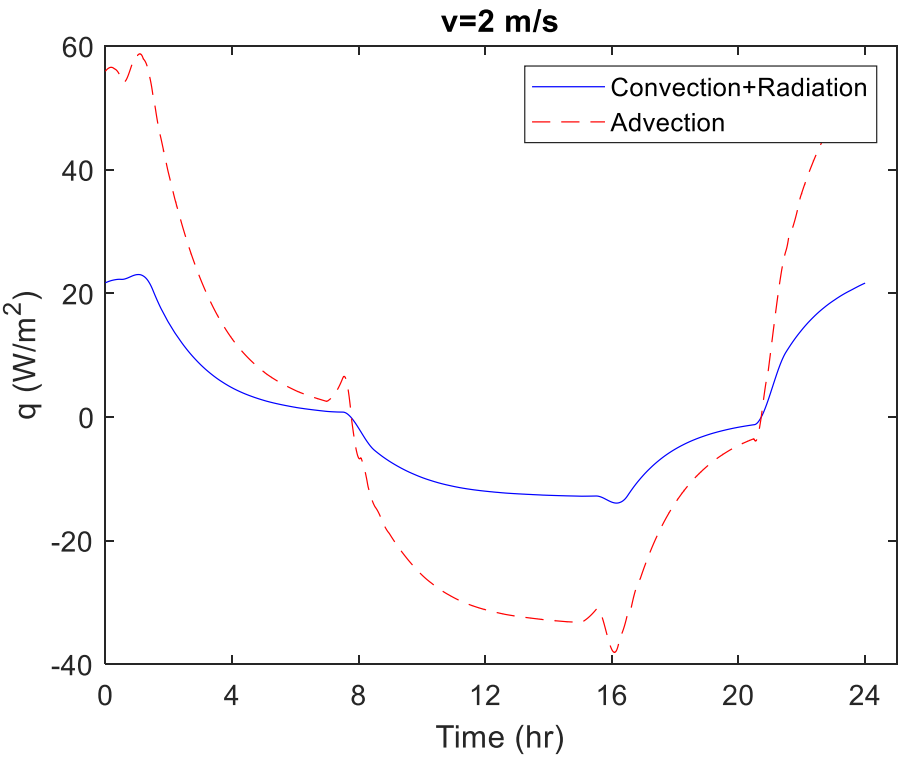


Figure 11. Heat flux density changes for an interior VBW over a 24-h period (positive values mean heat flows from the wall to the room).

Table 7 presents the minimum and maximum heat flux densities for different zone temperature profiles and air speeds.

Table 7. Heat flux densities for interior VBW with cement plaster.

Zone Temperature (Min/Max) (°C)	Heat Transfer Mechanism	Heat Flux Density (Min/Max) (W/m^2)		
		v = 0 m/s	v = 1 m/s	v = 2 m/s
20/26	Convection and radiation	−30.6/38.9	−19/28.9	−14.4/23.9
	Advection	0	−34/35.6	−39.5/60
20/24	Convection and radiation	−20.3/27.3	−12.4/20.7	−9/16.9
	Advection	0	−20/25.6	−21.7/46.7
20/22	Convection and radiation	−10.5/15.3	−5.9/13.1	−4.6/11.5
	Advection	0	−8.5/16.7	−14.3/24.9

Interior walls are more affected by convection and radiation when it comes to heating and cooling, compared to exterior walls. Having analyzed the simulation results for

heat flux density, convection and radiation have a greater contribution to the overall heat flux density to the zone than advection, when air speed is less than 0.8 m/s. This is attributed to the fact that both surfaces of the interior wall are exposed to the zone air. This causes the convection and radiation heat flux densities to increase significantly, making them the dominant heat transfer mechanisms over advection. However, when air speed exceeds 0.8 m/s, advection's share of the total heat flux density becomes greater than that of convection and radiation. Additionally, regardless of air speed, the wall continues to provide heat to the zone until 8 a.m. when the zone temperature is kept at 20 °C. In addition, the wall continues to deliver cooling energy to the zone until 8–9 p.m. as the temperature within the zone rises to 26 °C. There is a small heating contribution from the wall in the late night as the zone temperature decreases. For all zone temperature profiles, as the air speed increases, the advection heat flux density increases, while the convection and radiation heat flux densities decrease.

Net Energy Exchange

Table 8 presents the changes in net energy exchange based on different zone temperature profiles and air speeds for an interior wall.

Table 8. Net energy exchange of interior VBW with cement plaster.

Zone Temperature (Min/Max) (°C)	Net Energy Exchange (kWh/m^2)		
	v = 0 m/s	v = 1 m/s	v = 2 m/s
20/26	0.46	0.64	0.72
20/24	0.3	0.43	0.48
20/22	0.16	0.21	0.24

The net energy exchange for an interior VBW compared to an exterior VBW varies depending on air speed, with the potential to exchange 8–33% more energy for all zone air temperature profiles. However, as the peak temperatures within the zone decrease, the energy exchange also decreases by an average of 66%. This is because higher temperature rises within the zone allow for more efficient charging and discharging of thermal mass, which improves space heating and cooling.

Impact of Interior Finishing Layer on the Thermal Performance

To evaluate the influence of an interior surface finishing layer on the performance of an interior VBW, simulations were conducted at both passive performance (i.e., v = 0 m/s) and with an air speed of 2 m/s for all three typical-day zone air temperature profiles. Table 8 presented the simulation results for energy exchange values of an interior VBW with cement plaster as the interior finishing layer. Under passive performance, replacing the cement plaster layer with drywall reduced net energy exchange by an average of approximately 14% across all zone air temperature profiles. Additionally, at an air speed of 2 m/s, replacing cement plaster with drywall decreased net energy exchange by an average of approximately 9% for all zone air temperature profiles.

3.2. Annual Energy Analysis for VBW and Wood-Frame Wall

The impacts of VBWs and wood-frame walls on space heating and cooling loads are compared over the course of a year. To evaluate the thermal performance of a VBW versus a traditional wood-frame wall, two indicators of performance were introduced: assisting heating energy and assisting cooling energy for reducing space heating and cooling loads. These indicators refer to the amount of thermal energy stored in each wall that contributes to reduced space heating and cooling loads over the course of a year.

Using the outdoor temperature, the predicted indoor temperature (explained in the Section 2), and the thermal model developed in this study, the annual thermal performance

of the VBW was simulated and analyzed. Figure 12 depicts the outdoor temperature, predicted indoor temperature, and the VBW interior surface temperature for three representative days in winter. As illustrated in Figure 12, the outdoor temperature ranged from −32 °C to nearly −13 °C during the selected three-day period in winter. Indoor temperatures, however, were largely kept above 20 °C with mechanical space heating. The interior wall surface stayed between 17.8 °C and 18.2 °C due to significant heat loss through the back of the wall. In the absence of temperature variations within the zone, the wall does not contribute to heating or cooling of the zone, particularly when the outdoor temperature is below freezing.

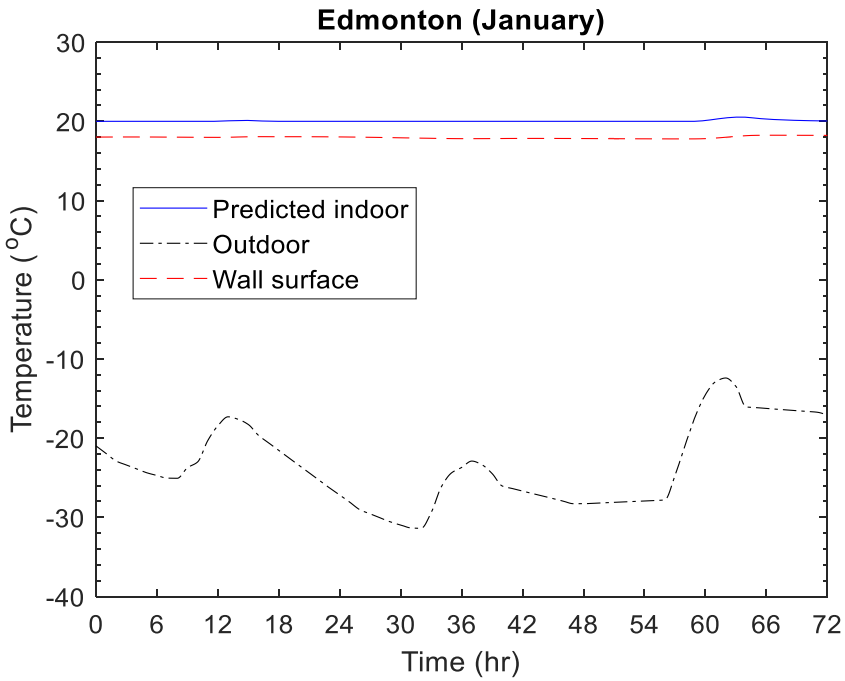


Figure 12. Outdoor, predicted indoor, and VBW surface temperatures for Edmonton, January.

Figure 13 illustrates the heat flux density of the VBW and wood-frame wall for three representative days in winter. As shown in Figure 13, both walls contributed to the unwanted cooling of the zone since their surface temperatures were lower than the zone temperature throughout the three-day period. Furthermore, the ventilation system was turned off for the entire time as the temperature of the VBW was below 20 °C. Therefore, the only heat exchange between the VBW and the zone occurred through the wall surface. The heat flux density for a wood-frame wall changed rapidly in response to indoor temperature changes, with a short time lag. However, the VBW's high thermal inertia meant that it took longer to observe temperature changes on the wall surface. For most hours, both walls had nearly identical surface temperatures, with a maximum temperature difference of 0.2 °C, due to minimal indoor temperature changes resulting in approximately the same heat flux density. However, between hours 59 and 63 in Figure 13 (i.e., 11 a.m. to 3 p.m. on the third day), the indoor temperature increased by approximately 0.7 °C due to a significant increase in outdoor temperature and solar radiation. Consequently, the wood-frame wall surface temperature increased rapidly due to changes in indoor and outdoor temperatures. Although the VBW's surface temperature also increased during those hours, the indoor temperature increased at a faster rate than the VBW temperature. Therefore, the VBW's heat flux density reached its minimum at hour 63 (i.e., a dive in the blue line in Figure 13) due to the higher temperature difference between the surface and the zone air.

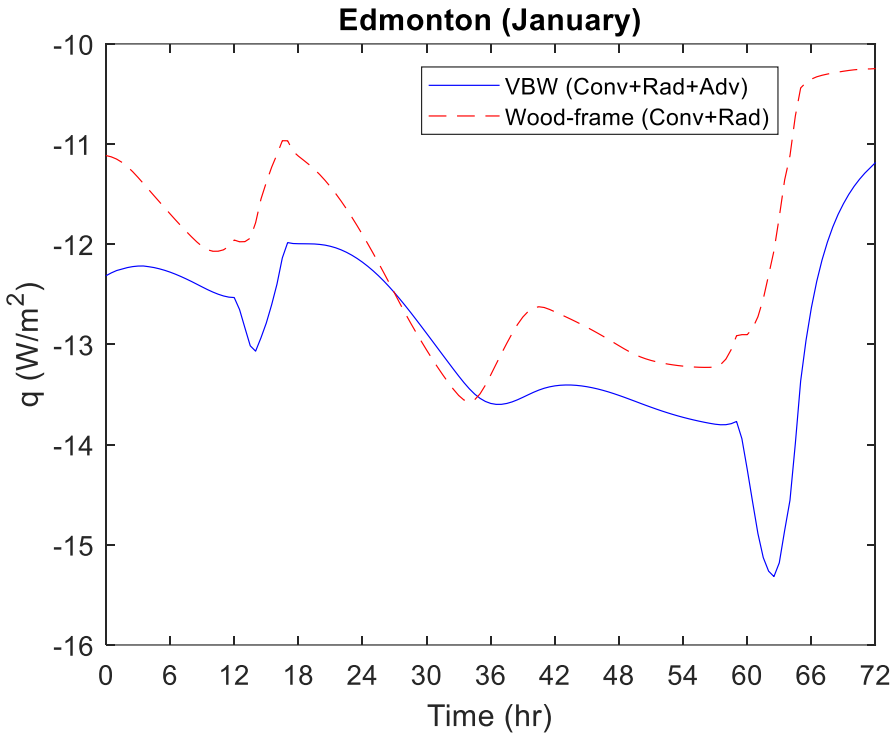


Figure 13. Heat flux density of the VBW and wood-frame wall for Edmonton, January (positive values mean heat flows from the wall to the room).

Figures 12 and 13 suggest that when the indoor temperature remains stable and outdoor temperature drops significantly during winter, both walls will provide little or no assisting heating energy.

During spring, summer, and fall, the walls show different behavior compared to winter due to greater variations in indoor temperature, higher outdoor temperature, and increased levels of solar radiation. Figure 14 shows the outdoor temperature, predicted indoor temperature, and surface temperature of the VBW for three representative days in summer. As depicted in Figure 14, outdoor temperatures are subject to large fluctuations in warm months. During the three-day period, the outdoor temperature varied between 7 °C and 23 °C. In most hours, this fluctuation in outdoor temperature caused the indoor temperature to fluctuate between 22.5 °C and 25 °C. The influence of variations in indoor temperature can be observed in the heating and cooling contributions of the VBW during the day. Heat storage within the VBW during hotter hours, when indoor temperature rises, can reduce space cooling demand. Subsequently, the VBW's high thermal inertia allows for the gradual release of heat during the cooler periods of the night and early morning, when indoor temperature decreases.

Figure 15 illustrates the heat flux density of the VBW and wood-frame wall for three representative days in summer. Figure 15 shows that the VBW contributes to space heating during the cool hours (i.e., early in the morning and late at night) and to space cooling during the warm hours (i.e., during the day when the solar radiation intensity is high), respectively. This implies that the space heating load can be reduced during the cooler hours, while the space cooling load can be reduced during the warmer hours, primarily due to the thermal storage capabilities of the VBW. Conversely, the exterior wood-frame wall cannot contribute to the heating of the zone compared to VBWs, especially in the cooling seasons. This is primarily due to the lack of ability to store thermal energy in wood-frame walls and the absence of an advection heat transfer mechanism. Indeed, advection plays a crucial role in the space heating and cooling at air speeds exceeding 0.3 m/s, as compared to convection and radiation. Significant zone temperature fluctuation enables more effective use of the thermal energy storage and release functions of the VBW.

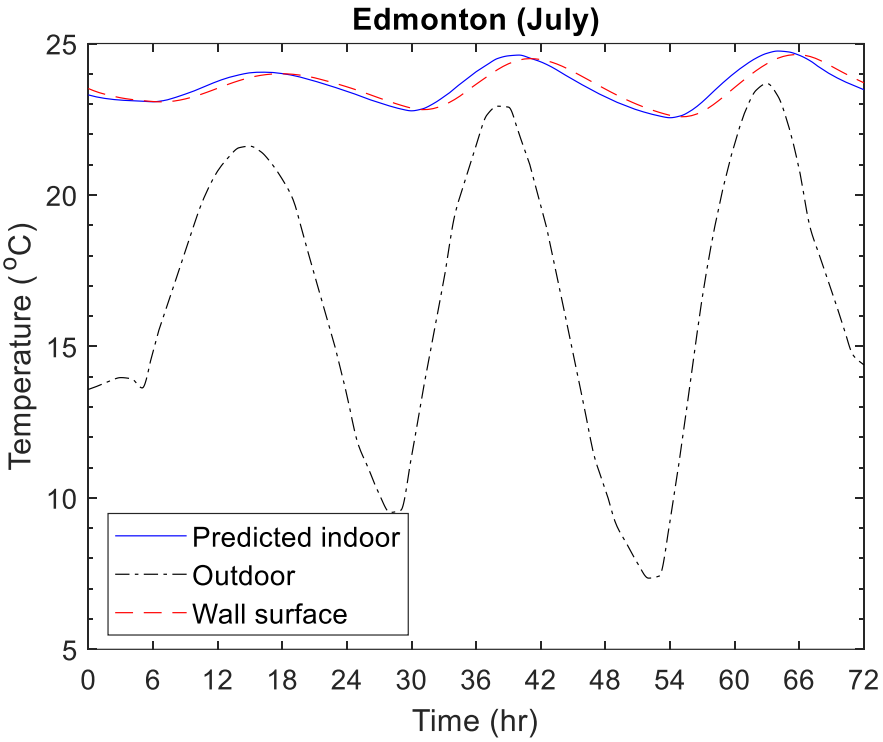


Figure 14. Outdoor, predicted indoor, and VBW surface temperatures for Edmonton, July.

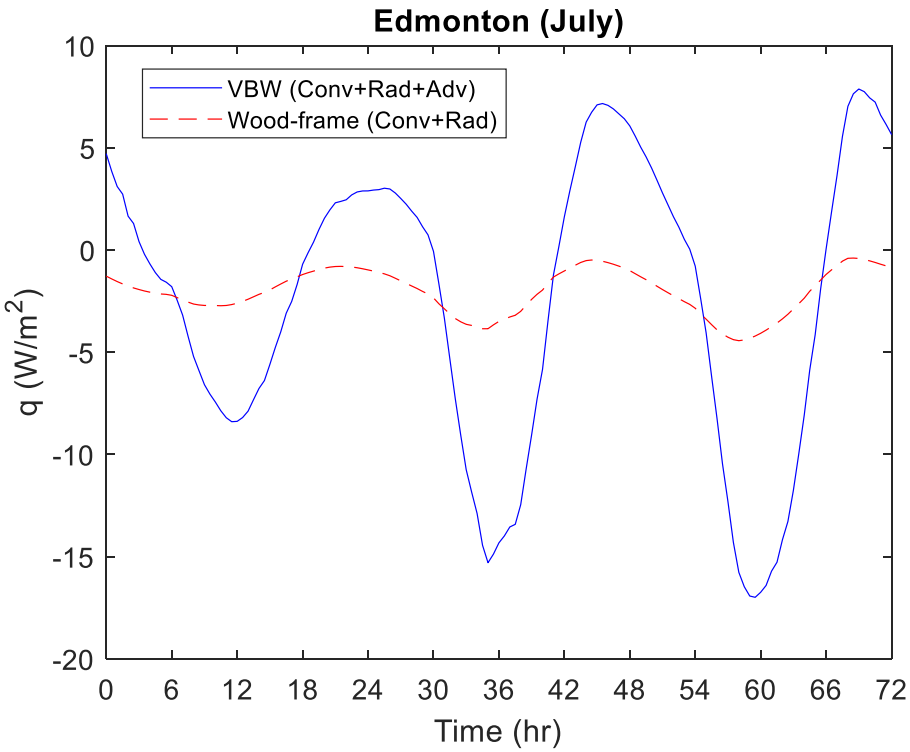


Figure 15. Heat flux density of the VBW and wood-frame wall for Edmonton, July (positive values mean heat from the walls to the room).

Table 9 presents the monthly assisting heating and cooling energy achieved by both walls for Edmonton (in a cold climate with large daily outdoor temperature fluctuation), based on the criteria defined in Table 2. These numbers show the reduction in space heating and cooling loads.

Table 9. Monthly total assisting heating and cooling energy achieved by both walls for Edmonton.

Month	Wood-Frame Wall			VBW					
				v = 2 m/s			v = 0 m/s		
	H * (kWh/m^2)	C #1 ** (kWh/m^2)	C #2 *** (kWh/m^2)	H (kWh/m^2)	C #1 (kWh/m^2)	C #2 (kWh/m^2)	H (kWh/m^2)	C #1 (kWh/m^2)	C #2 (kWh/m^2)
January	0	0	0	0.4	0	0	0	0	0
February	0	0	0	0.6	0	0	0	0	0
March	0	0	0	1	0	0	0	0	0
April	0.01	0	0	2.3	0	0.05	0.02	0	0.01
May	0.07	0.005	0.03	3	0.2	1.1	0.4	0.1	0.3
June	0.14	0.012	0.05	3.1	0.4	2.2	0.9	0.2	0.7
July	0.22	0.04	0.15	3.6	1.3	3.5	1.6	0.7	1.4
August	0.19	0.01	0.07	3.3	0.6	3	0.9	0.4	0.8
September	0.04	0.003	0.03	2.7	0.3	1.5	0.6	0.2	0.5
October	0.02	0	0	2.1	0	0.13	0.03	0	0.03
November	0	0	0	1.2	0	0	0	0	0
December	0	0	0	0.3	0	0	0	0	0
Total (kWh/m^2/year)	0.7	0.1	0.3	23.6	2.8	11.5	4.5	1.6	2.8
Fan energy consumption (kWh/year)		-			0.56			-	

* Heating. ** Cooling scenario #1. *** Cooling scenario #2.

Zone temperature fluctuation occurs as the outdoor temperature experiences lows and highs throughout the day, resulting in assisting heating energy from the walls when the zone temperature decreases and assisting cooling energy when the zone temperature rises. Across all months in a year, as shown in Table 9, July provides the most heating and cooling energy to the zone, largely due to the large zone temperature fluctuations around neutral temperature. Furthermore, cooling scenario #2 provides more cooling energy than scenario #1, owing to the less strict criteria in the calculation. Additionally, for Edmonton, the total assisting heating energy consistently exceeds the total assisting cooling energy, largely due to the very cold climate conditions in Edmonton, where the outdoor temperature is lower than 20 °C for most of the year.

The results in Table 9 demonstrate that a wood-frame wall has limited capacity to provide assisting heating and cooling energy (i.e., reduction in space heating and cooling), largely because its construction composition does not provide significant thermal mass to store and release heat during the day. Conversely, the VBW exhibits a notable capacity for assisting with heating and cooling energy in the zone, owing to its significant heat storage ability, as compared to a wood-frame wall. When using an air speed of 2 m/s for ventilation, replacing a wood-frame wall with a VBW leads to a reduction in space heating and cooling load by 35.1 kWh/m^2 (wall surface area) for Edmonton throughout the year. Passive performance (i.e., v = 0 m/s) results in a significant reduction in total heating and cooling energy when compared to an air speed of 2 m/s. Specifically, a reduction of 80%, 42%, and 74% was observed in total heating, total cooling in scenario #1, and total cooling in scenario #2, respectively. Tables similar to Table 9 for Vancouver and Toronto can be found in Appendix C.

According to the criteria outlined in Table 2, for assisting heating energy, the outdoor temperature needs to be lower than that of the zone, and the wall temperature should exceed the zone temperature. During the colder months (December to March) in Edmonton,

the assisting heating energy by VBW is minimal. This is due to the severe cold temperature outdoors, where it is rare for the wall temperature to surpass the zone temperature. In contrast, Vancouver, with its milder winter climate, often sees higher outdoor temperatures, causing the wall temperature to exceed the zone temperature more frequently than in Edmonton. Consequently, the total heating assistance in Vancouver during the colder months surpasses that of the two other cities. Toronto's winter coldness falls somewhere between that of Vancouver and Edmonton, with occasional extreme cold days and heavy snowfall. In these winter months, Toronto's heating energy assistance is more than Edmonton's but less than Vancouver's. However, during warm months, Edmonton's VBW contributes more heating energy to the zone due to larger daily temperature variations compared to Vancouver and Toronto. Edmonton's cool nights and hot days, sometimes with a temperature fluctuation near 20 °C, allow the VBW to absorb excess thermal energy during the day and release it at night and in the early morning when temperatures drop.

For cooling energy assistance scenarios, from October to April (the cold months), all three cities receive nearly zero cooling energy assistance, as the outdoor temperature remains below 20 °C most of the time. During the warm months (May to September), Toronto, due to its hotter and lengthier summer, provides more cooling energy to the zone compared to the other cities. This happens because there are more days when the outdoor temperature surpasses the zone temperature.

VBWs in cities with cold, dry climates and short summers such as Edmonton, coupled with high daily temperature fluctuations, result in a greater annual total of heating energy assistance. Toronto, with a cold, humid climate, milder winters, and longer summers, has slightly less heating assistance from the VBW compared to Edmonton. However, Toronto's total cooling energy assistance is 34% higher than Edmonton's. In cities with a moderate oceanic climate such as Vancouver, characterized by short summers and numerous overcast days, the VBW provides less total heating and cooling energy assistance throughout the year.

4. Conclusions

This study aimed to evaluate the thermal performance of a VBW with room air circulation by calculating the average wall temperature, the heat flux density from and to the wall, and the amount of energy that could be saved by using VBWs. The performance was assessed using two main approaches: (1) the typical-day thermal performance of a VBW under different boundary conditions, zone temperatures, and air speeds; and (2) the energy analysis and comparison of an exterior VBW and a traditional wood-frame wall over a one-year period with emphasis on a cold climate. Findings for the typical-day approach were investigated based on a parametric analysis of the zone temperature profile and air speed to determine their effect on the thermal performance of a VBW. Typical-day analysis revealed that, by increasing the air speed, the heat exchange between the VBWs and the zone could be increased. In addition, when the air speed was increased from 0 m/s to 2 m/s for an exterior VBW, thermal energy storage rose by 67% for any given zone temperature. In a similar manner, the net energy exchange for the interior VBW went up by 22% on average when the air speed rose from 0 m/s to 2 m/s. For all temperature profiles, an interior VBW can save 8–33% more energy than an exterior VBW. Moreover, the simulation results of the annual energy analysis showed that substituting a traditional wood-frame wall with a VBW can yield total assisting heating and cooling energy of 35.1 kWh/m^2 (wall area) for Edmonton, Canada throughout the year.

The current research is primarily based on simulations and the validation relies on experimental data obtained from a similar system. While this approach provides valuable insights and accuracy, conducting an experimental study specifically tailored to the proposed VBW system would offer more robust validation. In cases where conducting an experimental study is not feasible, it would be beneficial to utilize other commercially available simulation software to verify the results obtained from the 3D model. This would provide an additional layer of confidence in the findings.

Author Contributions: The paper is authored and communicated by M.R., C.C.-N. and Y.C., with M.R. being responsible for developing the methodology and mathematical model and analyzing the data, while C.C.-N. and Y.C. contributed through conceptualization, supervision, and manuscript revisions. All authors have read and agreed to the published version of the manuscript.

Funding: This research was funded by Natural Sciences and Engineering Research Council of Canada (NSERC), grant number CRDPJ 528050-18, and Masonry Contractors Association of Alberta (MCAA).

Data Availability Statement: The data that support the findings of this study are available from the corresponding author, M.R., upon reasonable request.

Acknowledgments: The authors would like to thank Alexander Jordan for his contributions during the proofreading process of the manuscript.

Conflicts of Interest: The authors declare no conflict of interest.

Nomenclature

Abbreviations	
CV	Control volume
CV-RMSE	Coefficient of variation of root-mean square error
FF	Framing factor
GHG	Greenhouse gas
GHI	Global horizontal irradiance
HDD	Heating degree day
NECB	National Energy Code of Canada for Buildings
RH	Relative humidity
TES	Thermal energy storage
TMY	Typical meteorological year
VBW	Ventilated block wall
Symbols	
Δx	x direction length of each control volume [m]
Δy	y direction length of each control volume [m]
Δz	z direction length of each control volume [m]
ΔT	Difference between the maximum and minimum average wall surface temperature [°C]
ΔP	Static pressure generated by fan or loss [Pa]
F_{fr}	Friction factor
$\dot{m}$	Air mass flow rate [kg/s]
λ_{wall}	Wall thermal conductivity [W/mK]
λ_{air}	Air thermal conductivity [W/mK]
ρ_{air}	Air density [kg/m^3]
F_v	View factor
L	Length of each CV in contact with node f of the air inside the channel [m]
v	Air speed in the channel [m/s]
ϑ	Air kinematic viscosity [m^2/s]
σ	Stefan–Boltzmann constant [W/m^2.K^4]
ε	Emissivity
A_{AC}	Cross-sectional area of the air channel [m^2]
Cp_{air}	Air specific heat capacity [J/kg°C]
D_h	Hydraulic diameter [m]
E_{fan}	Fan energy consumption [kWh]
Gr	Grashof number

h_{air}	Air convective heat transfer coefficient inside the channel [W/m^{2}K]
h_{total}	Combined heat transfer film coefficient between zone air and wall surface [W/m^{2}K]
Nu	Nusselt number
Pr	Prandtl number
q	Heat flux density [W/m^2]
$Q_{advection}$	Heat flow rate between returning air from the air channel and the zone air [W]
$Q_{conduction}$	Heat flow rate between wall nodes [W]
$Q_{convection}$	Heat flow rate between air inside the channel and surrounding wall nodes [W]
$Q_{radiation}$	Heat flow rate between two facing wall nodes in contact with air [W]
$Q_{surface}$	Heat flow rate between zone air and nodes on the wall surface [W]
Ra	Rayleigh number
Re	Reynolds number
S	Wall thickness [m]
T_{AC}	Temperature of the air inside the air channel [°C]
T_{air}	Zone temperature [°C]
$T_{outdoor}$	Outdoor temperature [°C]
T_{wall}	Average wall surface temperature [°C]
V_{wall}	The volume of one control volume [m^3]

Appendix A. Wood-Frame Wall

The overall thermal resistance of a wood-frame wall is primarily determined by the framing factor (FF) and the applied insulations. The FF of a wood-frame wall corresponds to the ratio of the wood's surface area (studs, top plates, bottom plates, etc.) to the total wall's surface area. The FF can vary from 6.3% to more than 40% depending on the type of exterior wall and its components [45]. The actual wall FF is usually higher due to junction between walls or added pieces of wood with the purpose of increasing the safety margin. An average FF for a house is defined as the total wall's framing area divided by the total area of the walls. The average FF is recommended to be between 19% and 23% [45]. Typically, a higher FF can be achieved by increasing the openings in a wall. The Canadian Wood Council and Canadian Mortgage and Housing Corporation (CMHC) [46] suggest that, typically, about 15% of a wood-frame wall area should consist of the framing material, depending on stud spacing and layout. In this situation, the FF can be increased by reducing the space between studs and/or by using double bottom plates when the concrete topping is applied to the floor [47]. In some cases, the wall comprises cripples, window headers, studs, a bottom plate, and two top plates, whereas in other cases, king studs, door headers, T-walls, trimmers, and corners can be added to the wall. As a result, these components can significantly increase the framing factor.

Moreover, rigid or semi-rigid insulation (i.e., continuous insulation) at the back of the wall, and the use of 2 × 6 studs or in some cases 2 × 8 studs, would improve the thermal performance of these types of walls. According to the CMHC [46], rigid or semi-rigid insulation has proven to be the most cost-effective method of enhancing thermal performance and minimizing thermal bridges.

In this study, an exterior wood-frame wall (2 × 6 nominal size, 1.5 × 5.5 actual size) with double top plates, one bottom plate, and studs spaced at 16 inches on-center was modeled. An FF of 13% was calculated for the modeled wall. Figure A1 shows the front view of the wood-frame wall (i.e., wood frame and insulation) and its discretization in three directions.

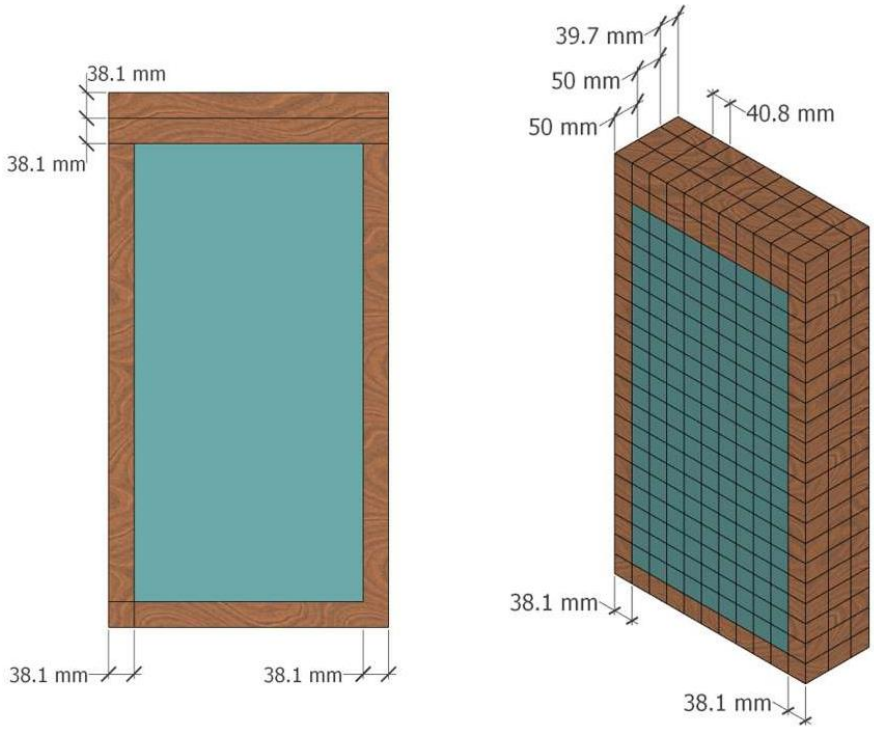


Figure A1. Front view of the wood-frame wall and its discretization in three directions.

As shown in Figure A1, the length of all the CVs in the studs is the same, however, it differs from the length of other CVs in the plates and insulation. Additionally, the heights of all CVs in the top and bottom plates are equal, but different from the height of all other CVs. The discretization of other continuous layers (i.e., drywall, plywood, and rigid insulation) is identical to the discretization shown in Figure A1. A schematic of the wood-frame wall is depicted in Figure A2.

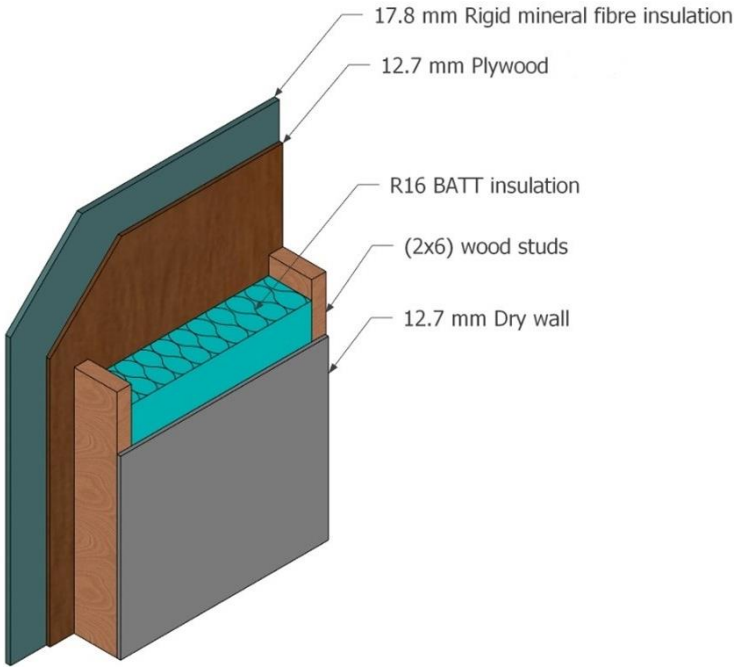


Figure A2. A schematic of the wood-frame wall.

The isothermal plane and parallel methods were utilized to determine the effective RSI value of the wood-frame wall [21]. Initially, the RSI value of the wood studs and insulation in the cavity was determined using the parallel method and, subsequently, the value was combined with RSI values of the remaining layers (isothermal plane method) to obtain the effective RSI value of the wood-frame wall.

The thermal resistance of the wood stud and insulation can be obtained using Equation (A1).

$$RSI_{wood-insulation} = \frac{1}{\frac{FF}{RSI_{wood}} + \frac{1-FF}{RSI_{insulation}}} \quad \text{(A1)}$$

where FF is the framing factor (i.e., 0.13), RSI_{wood} is the thermal resistance of the wood studs, and $RSI_{insulation}$ is the thermal resistance of the insulation placed in the cavity. The effective RSI value of the entire wall can be determined using Equation (A2).

$$RSI_{effective} = RSI_{Drywall} + RSI_{wood-insulation} + RSI_{Plywood} + RSI_{Rigidinsulation} \quad \text{(A2)}$$

Appendix B. Predicted and Measured Indoor Temperatures in Annual Energy Analysis

Figures A3–A5 compare the predicted indoor temperature with measured indoor temperature of the EcoTerra house for some typical days.

Figures A3–A5 demonstrate a strong correlation between the predicted indoor temperature data and the recorded indoor temperature data from the EcoTerra house.

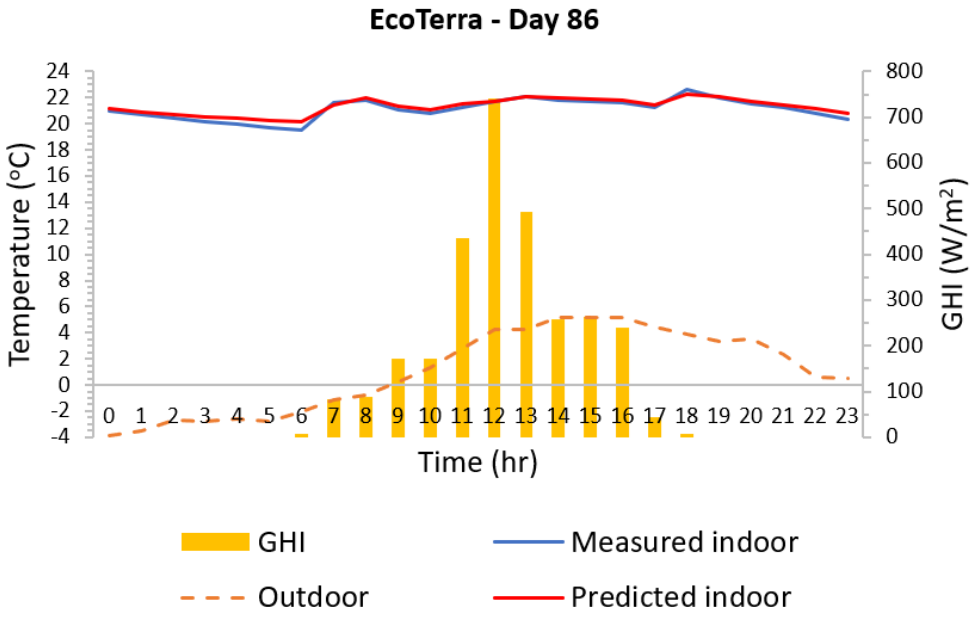


Figure A3. Measured and predicted average indoor temperature for EcoTerra house—day 86.

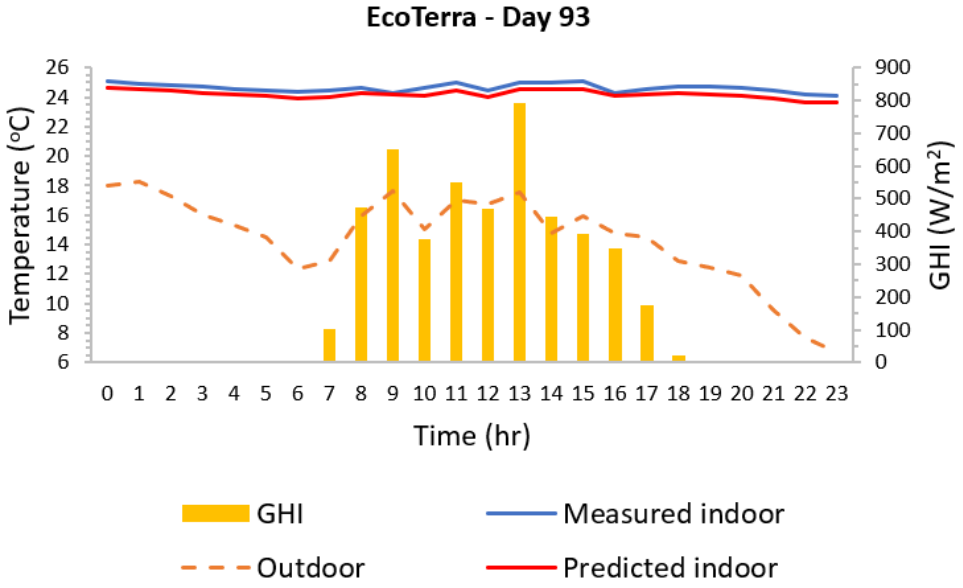


Figure A4. Measured and predicted average indoor temperature for EcoTerra house—day 93.

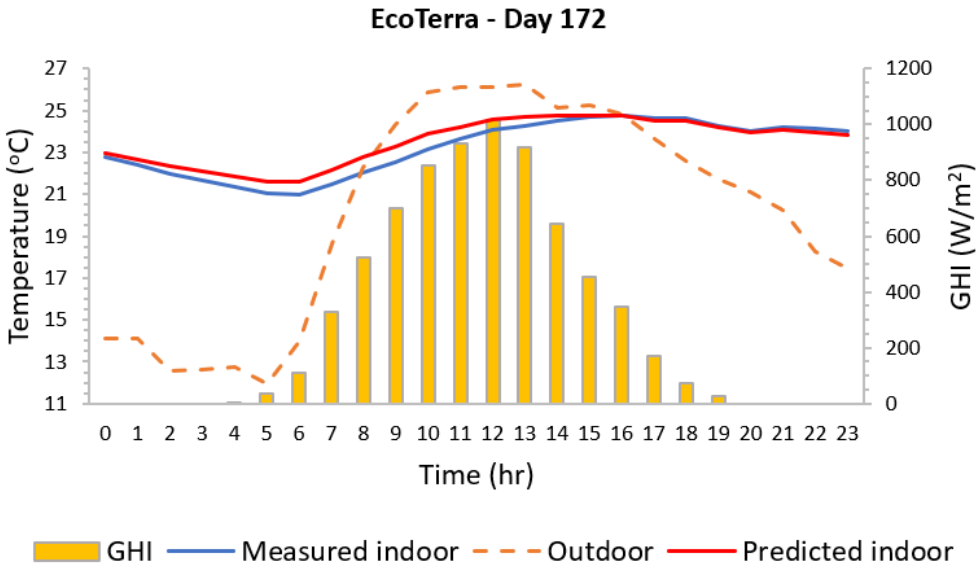


Figure A5. Measured and predicted average indoor temperature for EcoTerra house—day 172.

Appendix C. Annual Energy Analysis for Vancouver and Toronto

(a) Vancouver

Vancouver is located in the west of Canada and is known for its mild, oceanic climate. In the following, the main findings from the plots and tables are explained. Figure A6 depicts the outdoor temperature, predicted indoor temperature, and the VBW surface temperature for three representative days in winter.

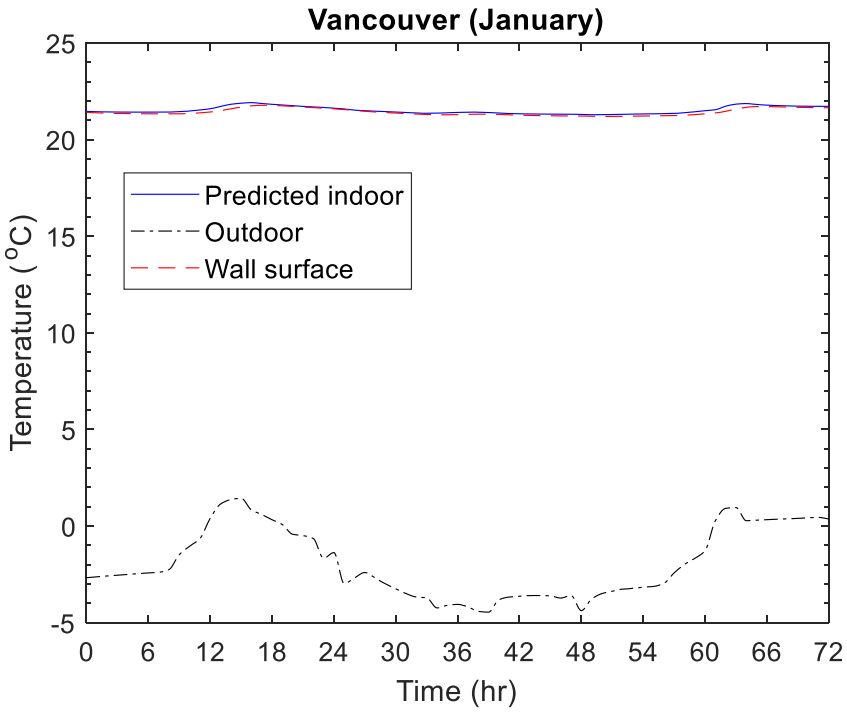


Figure A6. Outdoor, predicted indoor, and VBW surface temperatures for Vancouver, January.

Winters in Vancouver are warmer than those in Edmonton. In Figure A6, the wall surface temperature is lower than the indoor temperature during the sunny hours when the indoor temperature began to rise, resulting in cooling contributions. However, during the cold hours of the day, neither cooling nor heating contributions were made.

Figure A7 shows the heat flux density of the VBW and wood-frame wall for three representative days in winter.

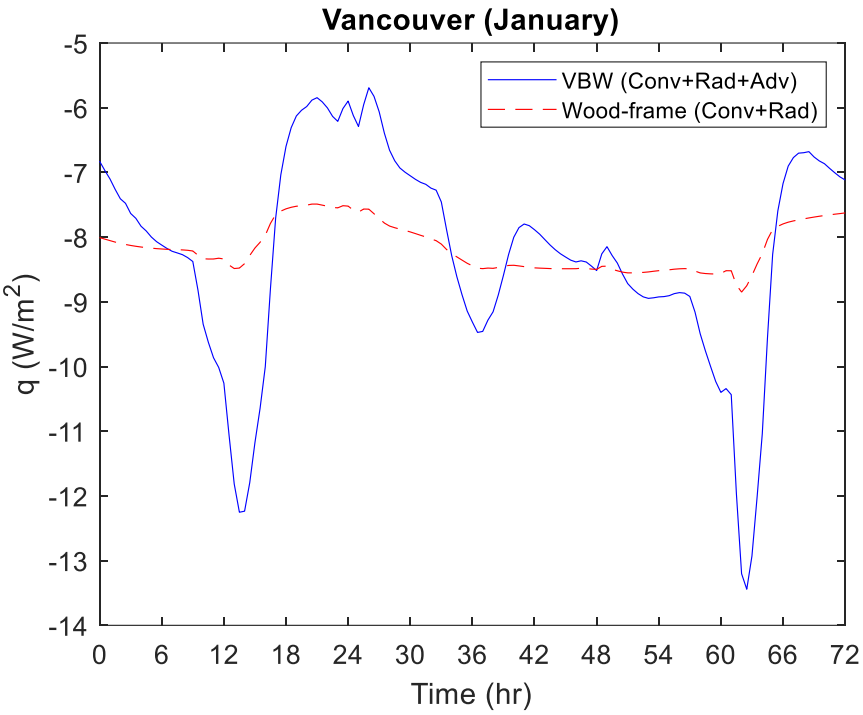


Figure A7. Heat flux density of the VBW and wood-frame wall for Vancouver, January.

Figure A7 shows that the VBW and wood-frame wall both contribute to cooling the zone during the entire three-day period. Nevertheless, the VBW provided more cooling during the sunny hours than the wood-frame wall due to its higher storage capacity and the significant role played by advection. During cold hours, the VBW contributed a lower level of cooling than a wood-frame wall. Given that the wall temperature remains consistently above 20 °C over the course of three days, the ventilation switches on and operates continuously. Consequently, during periods of increased temperature difference between the indoor environment and the wall, such as from hours 9 to 17 and hours 59 to 66, the heat flux density of the VBW falls to more negative values in comparison to a wood-frame wall, owing to the predominant influence of advection on total heat flux density compared to the convection and radiation.

Figure A8 illustrates the outdoor temperature, predicted indoor temperature, and the VBW surface temperature for three representative days in summer.

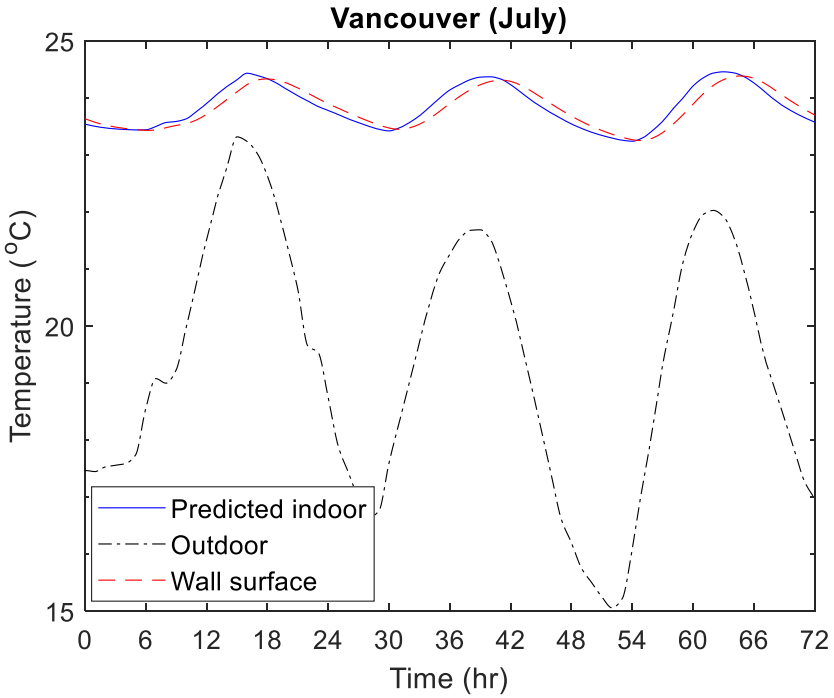


Figure A8. Outdoor, predicted indoor, and VBW surface temperatures for Vancouver, July.

As a result of more significant fluctuations in the outdoor temperature, the indoor temperature experiences pronounced swings throughout the day. Figure A8 shows heating contributions during cold hours and cooling contributions during sunny hours.

Figure A9 shows the changes in heat flux density for the VBW and wood-frame wall in Vancouver, for three representative days in summer.

The wood-frame wall only provided a small amount of cooling energy to the zone for the entire three-day period as shown in Figure A9. The VBW, however, contributed a significant amount of heating and cooling during the day, which assisted in better regulation of the zone temperature during the day.

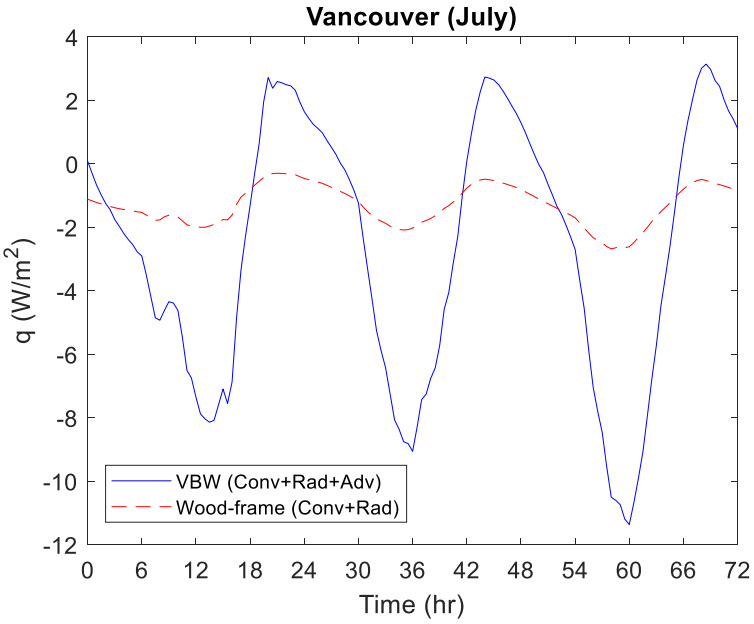


Figure A9. Heat flux density of VBW and wood-frame wall for Vancouver, July.

Table A1 presents the monthly total assisting heating and cooling energy achieved by both walls for Vancouver. These numbers show the reduction in space heating and cooling loads.

Table A1. Monthly total assisting heating and cooling energy achieved by both walls for Vancouver.

Month	Wood-Frame Wall			VBW					
				v = 2 m/s			v = 0 m/s		
	H * (kWh/m^2)	C #1 ** (kWh/m^2)	C #2 *** (kWh/m^2)	H (kWh/m^2)	C #1 (kWh/m^2)	C #2 (kWh/m^2)	H (kWh/m^2)	C #1 (kWh/m^2)	C #2 (kWh/m^2)
January	0	0	0	0.8	0	0	0	0	0
February	0	0	0	1	0	0	0	0	0
March	0	0	0	1.4	0	0	0	0	0
April	0.005	0	0	1.8	0	0.03	0.004	0	0.01
May	0.05	0	0	2.1	0	0.7	0.2	0	0.15
June	0.1	0.01	0.03	2.3	0.3	1.3	0.5	0.3	0.4
July	0.2	0.04	0.09	2.9	0.7	2.8	1.1	0.6	1
August	0.2	0.03	0.07	2.7	0.7	2.6	1	0.4	1
September	0.1	0.001	0.001	1.9	0.01	1.1	0.1	0.02	0.04
October	0.01	0	0	1.3	0	0.13	0	0	0
November	0	0	0	1	0	0	0	0	0
December	0	0	0	0.9	0	0	0	0	0
Total (kWh/m^2/year)	0.4	0.1	0.2	20.1	1.7	8.7	2.9	1.3	2.5
Fan energy consumption (kWh/year)		-			0.77			-	

* Heating. ** Cooling scenario #1. *** Cooling scenario #2.

Across all months in a year, as shown in Table A1, July provides the most heating and cooling energy to the zone, largely due to the heightened temperature fluctuations within the zone during this month. Furthermore, similar to Edmonton, cooling scenario #2 provides more cooling energy than scenario #1. Moreover, in Vancouver, fan energy consumption is greater than in Edmonton, as the fan is operated for more hours throughout the year due to the wall temperature experiencing more hours above 20 °C compared to Edmonton.

When using an air speed of 2 m/s for ventilation, replacing a wood-frame wall with a VBW results in a decrease in space heating and cooling loads by 28.8 kWh/m^2 (wall surface area) for Vancouver, Canada throughout the year. Passive performance (i.e., v = 0 m/s) results in a significant reduction in total heating and cooling energy when compared to an air speed of 2 m/s. Specifically, a reduction of 86%, 35%, and 70% was observed in total heating, total cooling in scenario #1, and total cooling in scenario #2, respectively.

(b) Toronto

Toronto is the capital city of Ontario, a province in eastern Canada. On average, Toronto enjoys more than 2000 h of bright sunshine each year, making it one of the top ten major cities in Canada in terms of sunny hours [48]. In contrast to Vancouver, Toronto has colder and longer winters.

For Toronto, merely the plots and the monthly total assisting heating and cooling energy values are presented. More discussion can be found in the related analyses for Edmonton and Vancouver.

Figure A10 shows the outdoor temperature, predicted indoor temperature, and the VBW surface temperature for three representative days in winter.

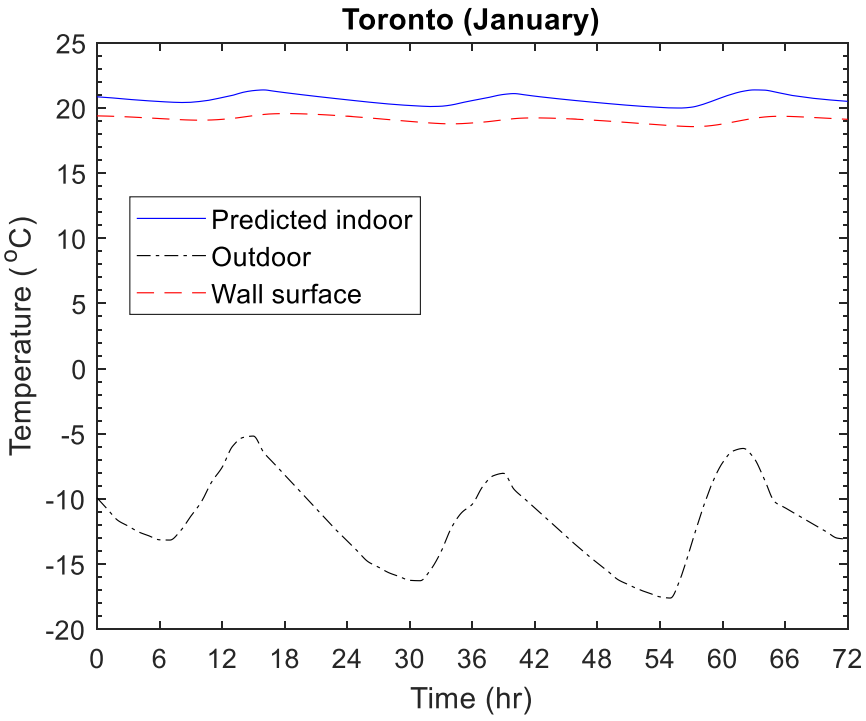


Figure A10. Outdoor, predicted indoor, and VBW surface temperatures for Toronto, January.

Figure A11 shows the changes in heat flux density for the VBW and wood-frame wall in Toronto, for three representative days in summer.

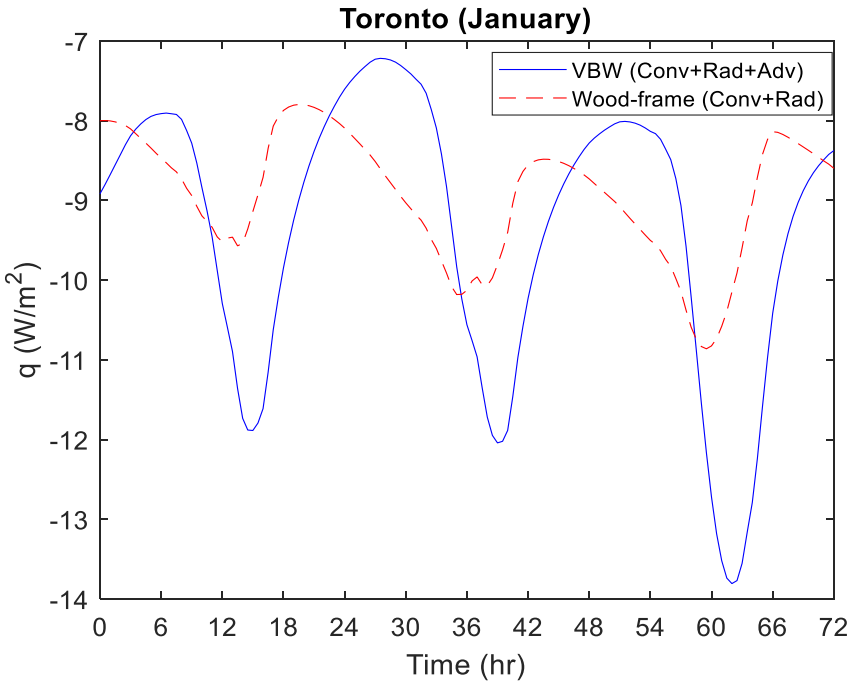


Figure A11. Heat flux density of the VBW and wood-frame wall for Toronto, January.

Figure A12 shows the outdoor temperature, predicted indoor temperature, and the VBW surface temperature for three representative days in summer.

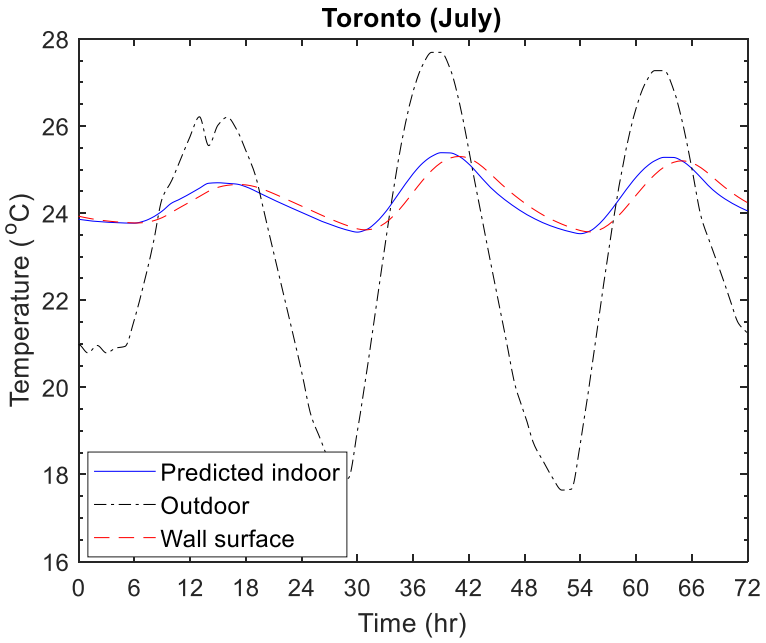


Figure A12. Outdoor, predicted indoor, and VBW surface temperatures for Toronto, July.

Figure A13 depicts the changes in heat flux density for the VBW and wood-frame wall in Toronto, for three representative days in summer.

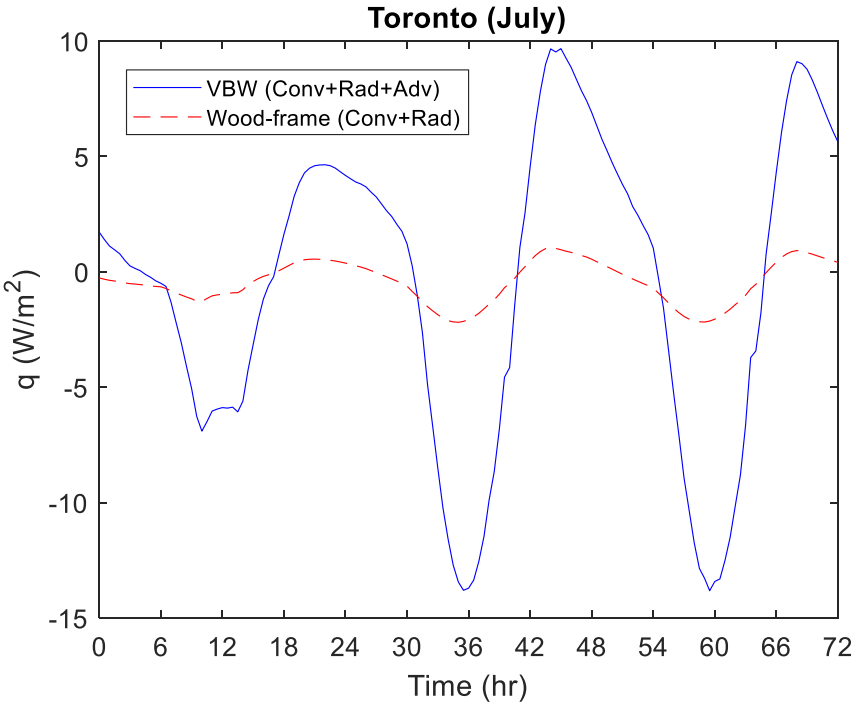


Figure A13. Heat flux density of VBW and wood-frame wall for Toronto, July.

Table A2 presents the monthly total assisting heating and cooling energy achieved by both walls for Toronto. These numbers show the reduction in space heating and cooling loads.

Table A2. Monthly total assisting heating and cooling energy achieved by both walls for Toronto.

Month	Wood-Frame Wall			VBW					
				v = 2 m/s			v = 0 m/s		
	H * (kWh/m^2)	C #1 ** (kWh/m^2)	C #2 *** (kWh/m^2)	H (kWh/m^2)	C #1 (kWh/m^2)	C #2 (kWh/m^2)	H (kWh/m^2)	C #1 (kWh/m^2)	C #2 (kWh/m^2)
January	0	0	0	0.8	0	0	0	0	0
February	0	0	0	0.9	0	0	0	0	0
March	0	0	0	1.6	0	0	0	0	0
April	0	0	0	1.8	0	0	0	0	0
May	0.05	0.01	0.03	2.6	0.3	1.5	0.06	0.03	0.05
June	0.1	0.04	0.07	2.9	0.8	3.2	0.3	0.2	0.4
July	0.2	0.09	0.15	2.9	2.8	4	1.3	1	1.3
August	0.2	0.05	0.1	2.9	2.3	3.7	1.2	0.7	1.1
September	0.05	0.03	0.07	2.3	0.7	2.3	0.9	0.2	0.6
October	0.02	0	0	1.5	0	0.13	0	0	0.03
November	0	0	0	1.2	0	0	0	0	0
December	0	0	0	1	0	0	0	0	0
Total (kWh/m^2/year)	0.6	0.2	0.4	22.4	6.9	14.8	3.8	2.2	3.5
Fan energy consumption (kWh/year)		-			0.72			-	

* Heating. ** Cooling scenario #1. *** Cooling scenario #2.

Across all months in a year, as shown in Table A2, July provides the most heating and cooling energy to the zone. In line with other cities, assisted cooling energy scenario #1 shows that the total amount is consistently lower than total heating energy. However, unlike Edmonton and Vancouver, Toronto's cooling energy scenario #2 reveals that cooling energy surpasses heating energy during the summer months of June, July, and August. This indicates that Toronto experienced numerous hours when outdoor temperatures exceeded 20 °C, and the VBW supplied cooling to the area during this period.

When using an air speed of 2 m/s for ventilation, replacing a wood-frame wall with a VBW leads to a reduction in space heating and cooling load by 37.2 kWh/m^2 (wall surface area) for Toronto, Canada throughout the year. Passive performance (i.e., v = 0 m/s) results in a significant reduction in total heating and cooling energy when compared to an air speed of 2 m/s. Specifically, a reduction of 80%, 42%, and 74% was observed in total heating, total cooling in scenario #1, and total cooling in scenario #2, respectively.

Appendix D. A Typical-Day Performance with Drywall as the Interior Surface Finishing

In this appendix, the results for the typical-day performance of the VBW with drywall as the interior surface finishing are presented. The following figures are associated with the exterior VBW when considering an air speed of 2 m/s and peak zone air temperature of 26 °C.

Figure A14 shows the average wall surface temperature. Results for other scenarios are tabulated in Table A3.

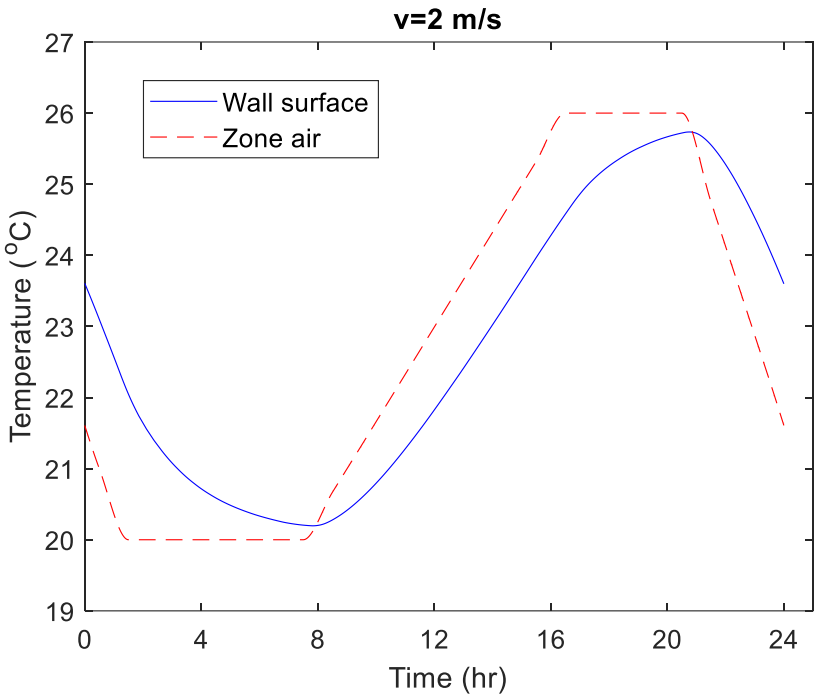


Figure A14. Zone air and average wall surface temperatures for an exterior VBW with drywall finishing.

Table A3. Maximum and minimum average wall interior surface temperatures for different zone temperatures and air speeds—drywall as the finishing layer.

Zone Temperature (Min/Max) (°C)	Average Wall Surface Temperature (°C)								
	v = 0 m/s			v = 1 m/s			v = 2 m/s		
	Min	Max	Max−Min (ΔT)	Min	Max	Max−Min (ΔT)	Min	Max	Max−Min (ΔT)
20/26	21.12	24.0	2.88	20.40	25.40	5	20.13	25.7	5.57
20/24	21.0	22.9	1.9	20.24	23.52	3.28	20.30	23.90	3.6
20/22	20.37	21.51	1.14	20.3	21.7	1.4	20.18	21.9	1.72

Figure A15 shows heat flux density changes for VBW with drywall as the interior finishing. Table A4 shows the results for other scenarios.

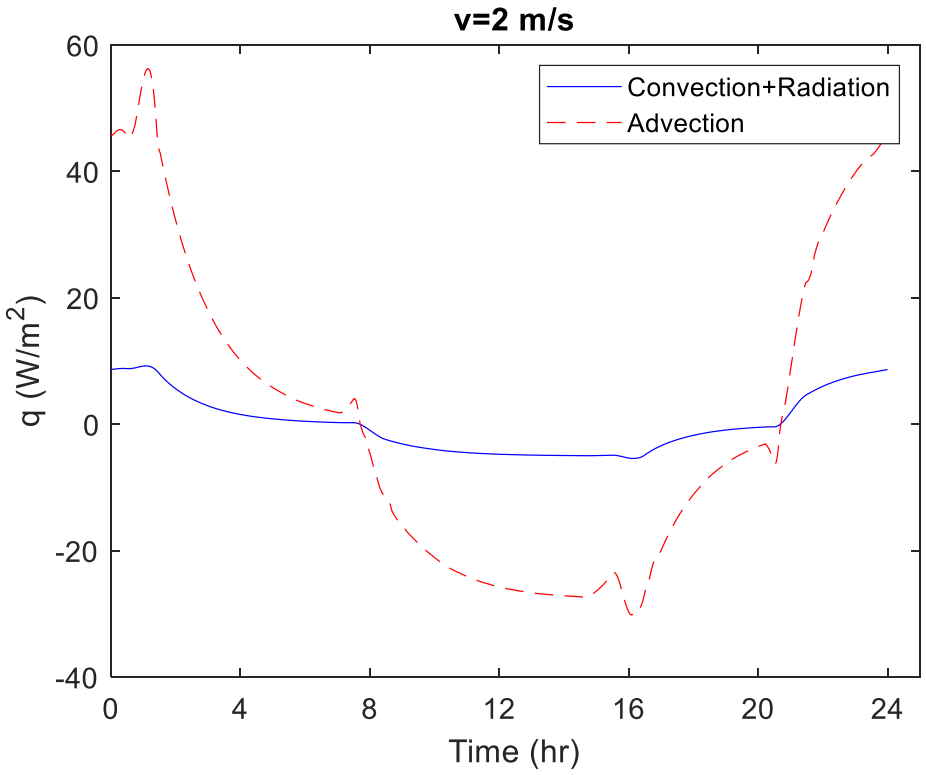


Figure A15. Heat flux density changes for an exterior VBW with drywall finishing over a 24-h period.

Table A4. Heat flux density for an exterior VBW—drywall as the finishing layer.

Zone Temperature (Min/Max) (°C)	Heat Transfer Mechanism	Heat Flux Density (Min/Max) (W/m^2)		
		v = 0 m/s	v = 1 m/s	v = 2 m/s
20/26	Convection and radiation	−13/13.7	−8/11.7	−5.4/9.1
	Advection	0	−26.5/39.1	−30.1/55.2
20/24	Convection and radiation	−8.3/10.1	−5.2/8.5	−3.6/6.7
	Advection	0	−19.3/29.3	−20/35.6
20/22	Convection and radiation	−4.2/6.2	−2.6/5.4	−2/4.7
	Advection	0	−10.1/16.5	−15.9/24.2

Table A5 presents the net energy exchange between VBW and zone when drywall was selected as the interior finishing layer.

Table A5. Net energy exchange of the exterior VBW—drywall as the finishing layer.

Zone Temperature (Min/Max) (°C)	Net Energy Exchange (kWh/m^2)		
	v = 0 m/s	v = 1 m/s	v = 2 m/s
20/26	0.17	0.43	0.51
20/24	0.11	0.29	0.35
20/22	0.05	0.15	0.19

References

1. Lacroix, G.; Moreau, A.; Haghighat, F.; Olsthoorn, D. Abilities and limitations of thermal mass activation for thermal comfort, peak shifting and shaving: A review. *Build. Environ.* **2017**, *118*, 113–127.
2. Levesque, A.; Pietzcker, R.; Baumstark, L.; De Stercke, S.; Grubler, A.; Luderer, G. How much energy will buildings consume in 2100? A global perspective within a scenario framework. *Energy* **2018**, *148*, 514–527. [CrossRef]
3. Levesque, A.; Pietzcker, R.C.; Luderer, G. Halving energy demand from buildings: The impact of low consumption practices. *Technol. Forecast. Soc. Chang.* **2019**, *146*, 253–266. [CrossRef]
4. Heier, J.; Bales, C.; Martin, V. Combining thermal energy storage with buildings—A review. *Renew. Sustain. Energy Rev.* **2015**, *42*, 1305–1325. [CrossRef]
5. De Gracia, A.; Cabeza, L.F. Phase change materials and thermal energy storage for buildings. *Energy Build.* **2015**, *103*, 414–419. [CrossRef]
6. Dincer, I. On thermal energy storage systems and applications in buildings. *Energy Build.* **2002**, *34*, 377–388. [CrossRef]
7. Alva, G.; Lin, Y.; Fang, G. An overview of thermal energy storage systems. *Energy* **2018**, *144*, 341–378. [CrossRef]
8. Chen, Y.; Galal, K.E.; Athienitis, A.K. Integrating hollow-core masonry walls and precast concrete slabs into building space heating and cooling. *J. Build. Eng.* **2016**, *5*, 277–287. [CrossRef]
9. Bouvenot, J.-B.; Egg, M. Numerical and Experimental Study of A Supply Air Wall Based on Integrated Insulation Clay Hollow Blocks. *J. Phys. Conf. Ser.* **2021**, *2069*, 012099. [CrossRef]
10. Huang, J.; Yu, J.; Yang, H. Effects of key factors on the heat insulation performance of a hollow block ventilated wall. *Appl. Energy* **2018**, *232*, 409–423. [CrossRef]
11. Yu, J.; Yang, J.; Xiong, C. Study of dynamic thermal performance of hollow block ventilated wall. *Renew. Energy* **2015**, *84*, 145–151. [CrossRef]
12. Yu, T.; Zhao, J.; Zhou, J.; Lei, B. Experimental and numerical studies on dynamic thermal performance of hollow ventilated interior wall. *Appl. Therm. Eng.* **2020**, *180*, 115851. [CrossRef]
13. Bunn, R. Termodeck: The thermal flywheel. *Build. Serv. Eng. Res. Technol.* **1991**, *13*, 41–44.
14. Labat, M.; Hazyuk, I.; Cezard, M.; Lorente, S. Indoor thermal behaviour of an office equipped with a ventilated slab: A numerical study. *J. Build. Perform. Simul.* **2021**, *14*, 227–246. [CrossRef]
15. Chen, Y.; Galal, K.E.; Athienitis, A.K. Athienitis, Design and operation methodology for active building-integrated thermal energy storage systems. *Energy Build.* **2014**, *84*, 575–585. [CrossRef]
16. Barnaby, C.; Nall, D.; Dean, E. Structural mass cooling in a commercial building using hollowcore concrete plank. *Proc. Annu. Meet.Am. Sect. Int. Sol. Energy Soc.* **1980**, *5*, 2.
17. Russell, M.; Surendran, P. Influence of active heat sinks on fabric thermal storage in building mass. *Appl. Energy* **2001**, *70*, 17–33. [CrossRef]
18. Zmeureanu, R.; Fazio, P. Thermal performance of a hollow core concrete floor system for passive cooling. *Build. Environ.* **1988**, *23*, 243–252. [CrossRef]
19. Zhou, J.; Yu, T.; Lei, B. Experimental study on the influence of solar heat gain on the thermal performance of hollow ventilated interior wall. *J. Sol. Energy Eng.* **2022**, *144*, 1–34. [CrossRef]
20. Canadian Concrete Masonry Producers' Association (CCMPA). Empirical Masonry Design Guidelines. Available online: https://ccmpa.ca/wp-content/uploads/2012/02/8-EmprclMsnryDsgn.pdf (accessed on 8 October 2022).
21. The National Research Council of Canada. *National Energy Code of Canada for Buildings*; Government of Canada: Ottawa, ON, Canada, 2020.
22. ASHRAE. *ASHRAE Handbook-Fundamentals*; ASHRAE: Peachtree Corners, GA, USA, 2005.
23. Bisegna, F.; Mattoni, B.; Gori, P.; Asdrubali, F.; Guattari, C.; Evangelisti, L.; Sambuco, S.; Bianchi, F. Influence of Insulating Materials on Green Building Rating System Results. *Energies* **2016**, *9*, 712. [CrossRef]
24. Canadian Centre for Occupational Health and Safety (CCOHS). Temperature Condition at Workplace—Legislation. Available online: https://www.ccohs.ca/oshanswers/phys_agents/temp_legislation.html (accessed on 8 October 2022).

25. Jaakkola, J.; Heinonen, O.; Seppänen, O. Sick building syndrome, sensation of dryness and thermal comfort in relation to room temperature in an office building: Need for individual control of temperature. *Environ. Int.* **1989**, *15*, 163–168. [CrossRef]
26. Oetomo, A.; Jalali, N.; Costa, P.D.P.; Morita, P.P. Indoor Temperatures in the 2018 Heat Wave in Quebec, Canada: Exploratory Study Using Ecobee Smart Thermostats. *JMIR Form. Res.* **2022**, *6*, e34104. [CrossRef]
27. Ontario Regulation. Ontario Residential Tenancies Act. Available online: https://www.ontario.ca/laws/regulation/060516 (accessed on 8 October 2022).
28. Tham, S.; Thompson, R.; Landeg, O.; Murray, K.; Waite, T. Indoor temperature and health: A global systematic review. *Public Health* **2019**, *179*, 9–17. [CrossRef]
29. Masa, N.; Andreas, A.; Véronique, D.; Josef, A.; Bradley, B. *Net Zero Energy Homes of the Future: A Case Study of the EcoTerraTM House in Canada*; Renewable Energy Congress: Glasgow, UK, 2008.
30. Bergman, T.L.; Lavine, A.S.; Incropera, F.P.; DeWitt, D.P. *Introduction to Heat Transfer*; John Wiley & Sons: New York, NY, USA, 2011.
31. Travis, Q.B.; Mays, L.W. Relationship between hazen-william and colebrook-white roughness values. *J. Hydraul. Eng.* **2007**, *133*, 1270–1273. [CrossRef]
32. Chanson, H. *Hydraulics of Open Channel Flow*; Elsevier: Amsterdam, The Netherlands, 2004.
33. Tayşi, N.; Abid, S. Temperature distributions and variations in concrete box-girder bridges: Experimental and finite element parametric studies. *Adv. Struct. Eng.* **2015**, *18*, 469–486. [CrossRef]
34. Babiak, J.; Olesen, B.W.; Petras, D. *Low Temperature Heating and High Temperature Cooling: REHVA GUIDEBOOK No 7*; REHVA: Ixelles, Belgium, 2007.
35. *ISO 11855–2*; 2012 (E) Building Environment Design-Design, Dimensioning, Installation and Control of Embedded Radiant Heating and Cooling Systems. Part 2: Determination of the Design Heating and Cooling Capacity. International Organization for Standard: Geneve, Switzerland, 2012.
36. Shinoda, J.; Kazanci, O.B.; Tanabe, S.-I.; Olesen, B.W. A review of the surface heat transfer coefficients of radiant heating and cooling systems. *Build. Environ.* **2019**, *159*, 106156. [CrossRef]
37. Femp, M. *Guidelines: Measurement and Verification for Federal Energy Projects, Version 3.0*; Energy Efficiency and Renewable Energy: Washington, DC, USA, 2008.
38. Barton, P.; Beggs, C.; Sleigh, P. A theoretical study of the thermal performance of the TermoDeck hollow core slab system. *Appl. Therm. Eng.* **2002**, *22*, 1485–1499. [CrossRef]
39. Yang, J.; Yu, J.; Xiong, C. Heat Transfer Analysis of Hollow Block Ventilated Wall Based on CFD Modeling. *Procedia Eng.* **2015**, *121*, 1312–1317. [CrossRef]
40. Yu, J.; Huang, J.; Xu, X.; Ye, H.; Xiong, C.; Wang, J.; Tian, L. A semi-dynamic heat transfer model of hollow block ventilated wall for thermal performance prediction. *Energy Build.* **2017**, *134*, 285–294. [CrossRef]
41. Streeter, V.; WE, B.K. *Fluid Mechanics*; WCB McGraw-Hill Inc.: Boston, MA, USA, 1998.
42. Li, J.; Meng, X.; Gao, Y.; Mao, W.; Luo, T.; Zhang, L. Effect of the insulation materials filling on the thermal performance of sintered hollow bricks. *Case Stud. Therm. Eng.* **2018**, *11*, 62–70. [CrossRef]
43. Pierquet, P.; Bowyer, J.L.; Huelman, P. Thermal performance and embodied energy of cold climate wall systems. *For. Prod. J.* **1998**, *48*, 53.
44. Sassine, E.; Kinab, E.; Cherif, Y.; Antczak, E.; Nasrallah, M. Thermal performance of lightweight concrete applications in building envelopes in Lebanon. *Build. Simul.* **2021**, *14*, 1359–1375. [CrossRef]
45. Qasass, R.; Gorgolewski, M.; Ge, H. Timber framing factors in Toronto residential house construction. *Arch. Sci. Rev.* **2014**, *57*, 159–168. [CrossRef]
46. Canadian Mortgage Housing and Corporation (CMHC). Wood Frame Envelopes. Best Practice Guide: Building Technology. Available online: https://publications.gc.ca/site/eng/9.647239/publication.html (accessed on 1 March 2023).
47. Canadian Mortgage Housing and Corporation (CMHC). Canadian Wood-Frame House Construction. Available online: https://publications.gc.ca/site/eng/9.700100/publication.html (accessed on 1 March 2023).
48. CurrentResults. Sunniest Cities in Canada. Available online: https://www.currentresults.com/Weather-Extremes/Canada/sunniest-cities.php060516 (accessed on 18 November 2022).

Disclaimer/Publisher's Note: The statements, opinions and data contained in all publications are solely those of the individual author(s) and contributor(s) and not of MDPI and/or the editor(s). MDPI and/or the editor(s) disclaim responsibility for any injury to people or property resulting from any ideas, methods, instructions or products referred to in the content.